Lens Thickness Impact on the Performance of Conformal Miniaturized Arrays Designed through a Material-by-Design Approach

M. Salucci, G. Oliveri, N. Anselmi, and A. Massa

Abstract

This work deals with the conformal miniaturization of linear antenna arrays. A novel design methodology based on the Material-by-Design (*MbD*) paradigm is proposed. More precisely, the presented approach exploits a two-step quasi-conformal transformation optics (*QCTO*) algorithm in order to match linear arrays onto arbitrary surfaces. The synthesized meta-material lens, covering the conformal array, ensures that its radiation features are kept as much as possible equal to those of the reference antenna in free-space. Moreover, a source inversion (*SI*) strategy is adopted in order to achieve a reduction of the radiators in the final conformal arrangement. A study of the impact of the lens thickness on the achievable performance is presented, making use of full-wave simulations in order to carefully analyze the electromagnetic behavior of the synthesized radiating architectures.

1 Numerical Assessment

1.1 Validation vs. Lens Curvature (l) and Lens Thickness (s)

Input Parameters

- **Virtual & Physical Geometries**

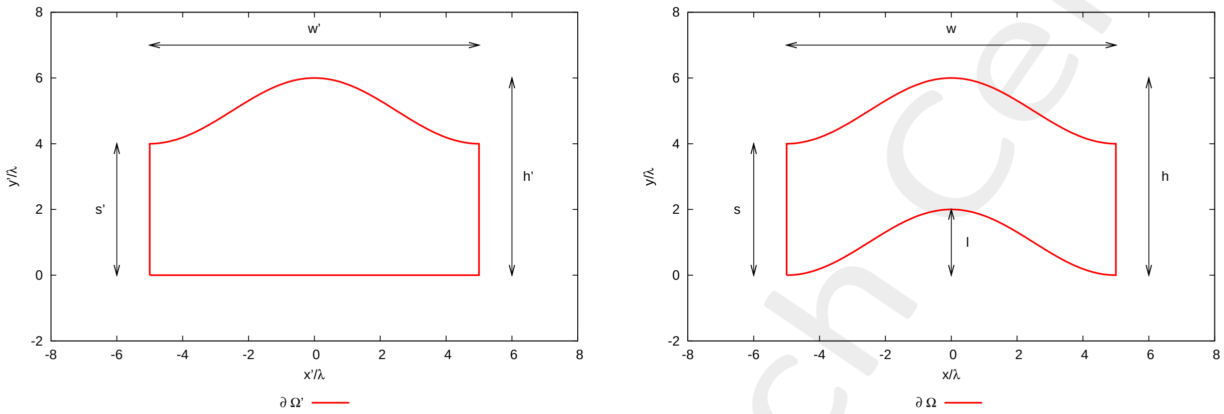

(a) (b)

Figure 1: Transformation regions and geometric parameters of interest.

Lens Thickness: $s = 4.0$ [λ]						
Virtual			**Physical**			
w' [λ]	h' [λ]	s' [λ]	w [λ]	h [λ]	s [λ]	l [λ] (Curvature)
16.0	4.5	4.0	16.0	4.5	4.0	**0.5**
16.0	5.0	4.0	16.0	5.0	4.0	**1.0**
16.0	5.5	4.0	16.0	5.5	4.0	**1.5**
16.0	6.0	4.0	16.0	6.0	4.0	**2.0**
Lens Thickness: $s = 2.0$ [λ]						
Virtual			**Physical**			
w' [λ]	h' [λ]	s' [λ]	w [λ]	h [λ]	s [λ]	l [λ] (Curvature)
16.0	2.5	2.0	16.0	2.5	2.0	**0.5**
16.0	3.0	2.0	16.0	3.0	2.0	**1.0**
16.0	3.5	2.0	16.0	3.5	2.0	**1.5**
16.0	4.0	2.0	16.0	4.0	2.0	**2.0**
Lens Thickness: $s = 1.0$ [λ]						
Virtual			**Physical**			
w' [λ]	h' [λ]	s' [λ]	w [λ]	h [λ]	s [λ]	l [λ] (Curvature)
16.0	1.5	1.0	16.0	1.5	1.0	**0.5**
16.0	2.0	1.0	16.0	2.0	1.0	**1.0**
16.0	2.5	1.0	16.0	2.5	1.0	**1.5**
16.0	3.0	1.0	16.0	3.0	1.0	**2.0**
Lens Thickness: $s = 0.5$ [λ]						
Virtual			**Physical**			
w' [λ]	h' [λ]	s' [λ]	w [λ]	h [λ]	s [λ]	l [λ] (Curvature)
16.0	1.0	0.5	16.0	1.0	0.5	**0.5**
16.0	1.5	0.5	16.0	1.5	0.5	**1.0**
16.0	2.0	0.5	16.0	2.0	0.5	**1.5**
16.0	2.5	0.5	16.0	2.5	0.5	**2.0**

Table I: Geometric descriptors for virtual and physical geometries. Note that $w' = w$, $h' = h$, $s' = s$, and $h = s + l$.

- **Virtual Array**
  - Number of elements, spacing, aperture: $N' = 20$, $d' = \frac{\lambda}{2}$, $L' = 9.5$ $[\lambda]$;
  - Distance from PEC ground plane (placed at $y' = 0.0$): $\delta' = \frac{\lambda}{4}$;
  - Operating frequency: $f = 600$ $[MHz]$;
  - Steering angle: $\phi_s = 90.0$ $[deg]$;
  - Excitations: $I_n = 1.0$, $\varphi_n = \frac{-2\pi}{\lambda} x_n sin\left(\phi_s + 90\right)$; $n = 1, ..., N'$;
- **QCTO**
  - Discretization cell dimension: 0.15 $[\lambda]$ (0.01 $[\lambda]$ for source mapping);

1.1.1 Results of the Transformation

Lens Thickness $s = 4.0$ $[\lambda]$

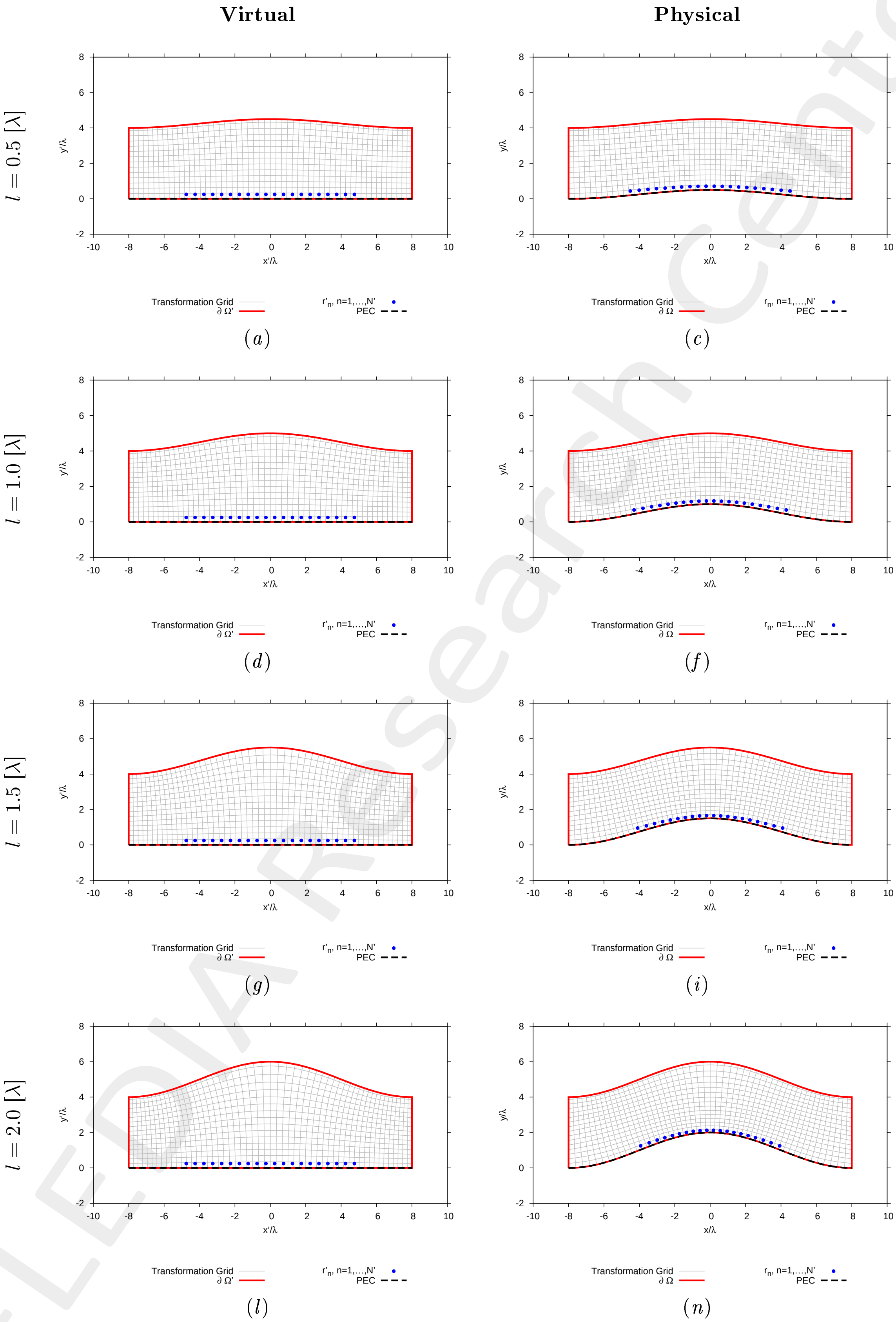

Figure 2: Lens thickness $s = 4.0$ $[\lambda]$ - Transformation grids for virtual and physical geometries for different curvatures of the lens.

Lens Thickness $s = 2.0$ $[\lambda]$

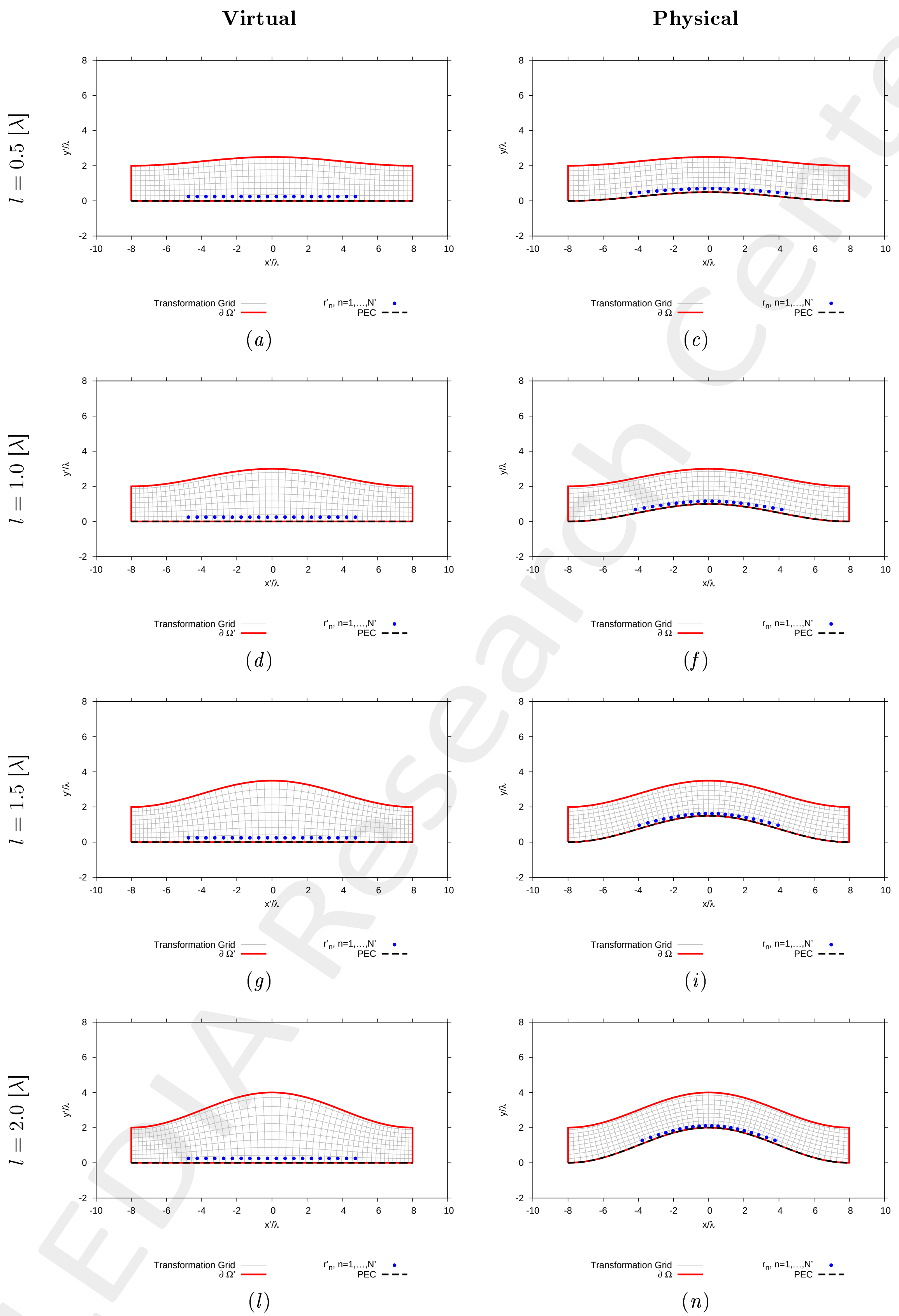

Figure 3: Lens thickness $s = 2.0$ $[\lambda]$ - Transformation grids for virtual and physical geometries for different curvatures of the lens.

Lens Thickness $s = 1.0$ [λ]

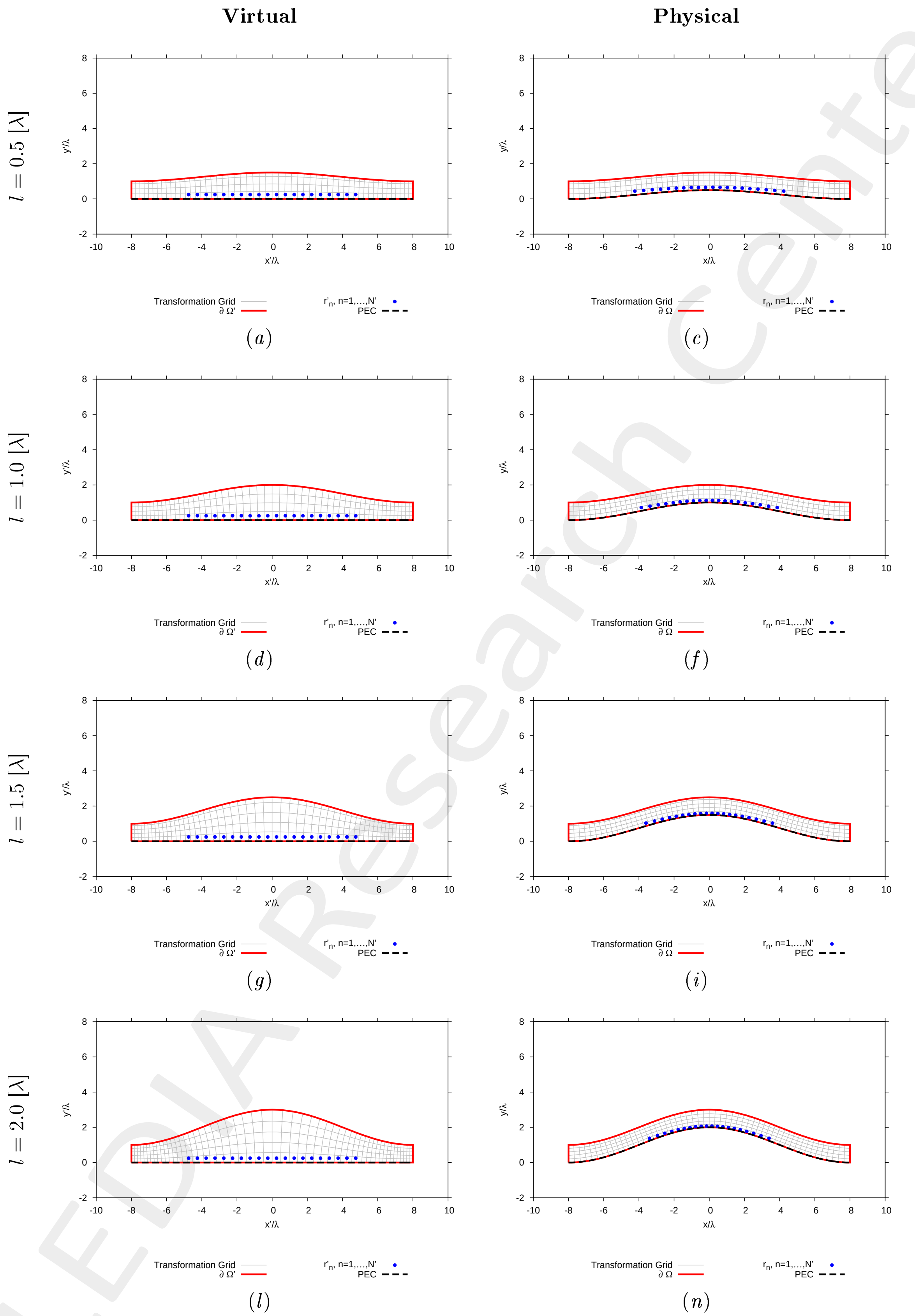

Figure 4: Lens thickness $s = 1.0$ [λ] - Transformation grids for virtual and physical geometries for different curvatures of the lens.

Lens Thickness $s = 0.5$ [λ]

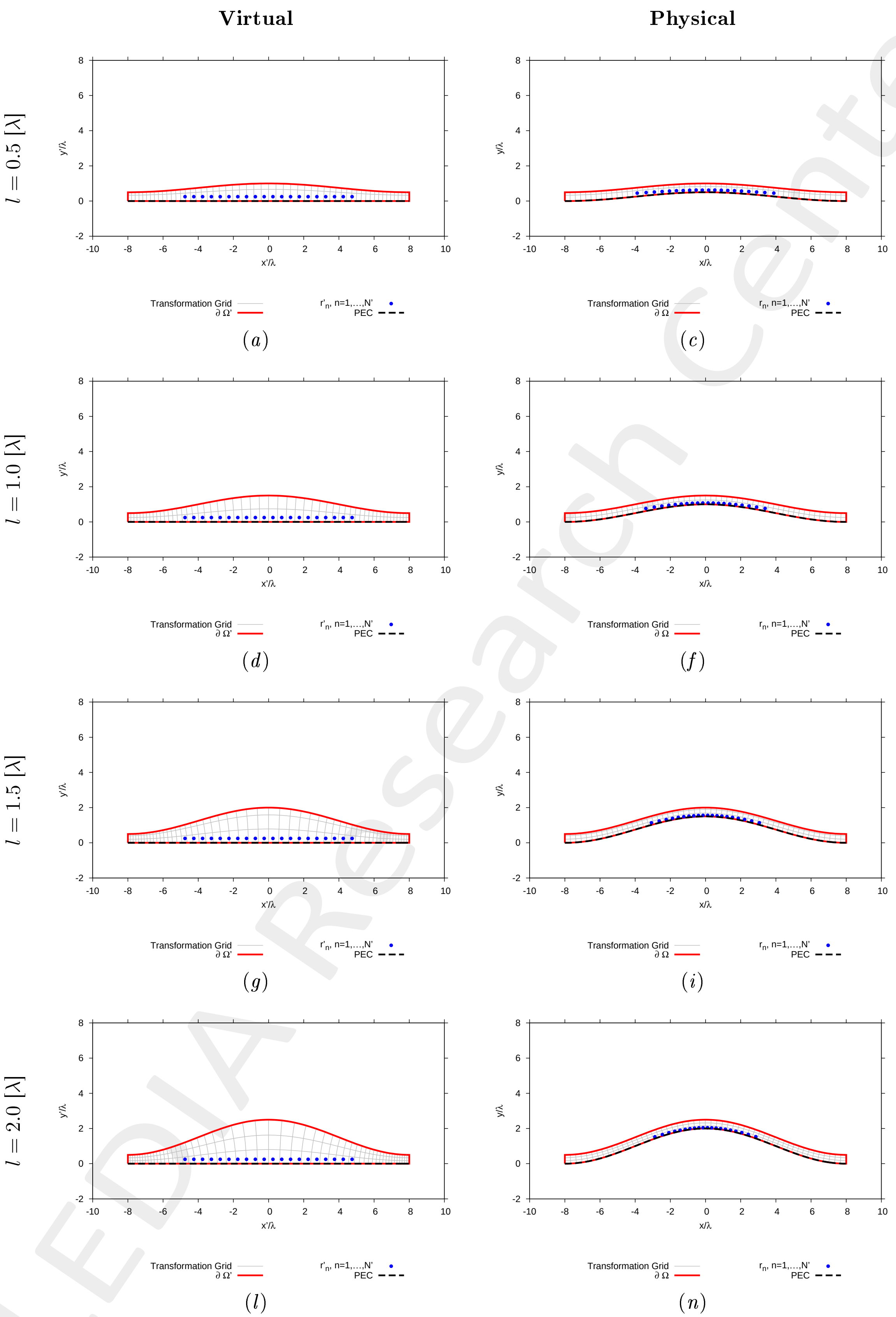

Figure 5: Lens thickness $s = 0.5$ [λ] - Transformation grids for virtual and physical geometries for different curvatures of the lens.

1.1.2 Physical Lens Parameters

Lens Curvature $l = 0.5$ [λ]				
	$s = 4.0$ [λ]	$s = 2.0$ [λ]	$s = 1.0$ [λ]	$s = 0.5$ [λ]
Anisotropic Permittivity Range	$[-0.030, 1.290]$	$[-0.030, 1.460]$	$[-0.060, 1.870]$	$[-0.110, 2.840]$
Isotropic Permittivity Range	$[0.00, 1.130]$	$[0.00, 1.160]$	$[0.00, 1.260]$	$[0.00, 1.440]$
Lens Curvature $l = 1.0$ [λ]				
	$s = 4.0$ [λ]	$s = 2.0$ [λ]	$s = 1.0$ [λ]	$s = 0.5$ [λ]
Anisotropic Permittivity Range	$[-0.070, 1.650]$	$[-0.100, 1.990]$	$[-0.170, 2.920]$	$[-0.280, 5.190]$
Isotropic Permittivity Range	$[0.00, 1.290]$	$[0.00, 1.340]$	$[0.00, 1.510]$	$[0.00, 1.810]$
Lens Curvature $l = 1.5$ [λ]				
	$s = 4.0$ [λ]	$s = 2.0$ [λ]	$s = 1.0$ [λ]	$s = 0.5$ [λ]
Anisotropic Permittivity Range	$[-0.120, 2.060]$	$[-0.200, 2.620]$	$[-0.320, 4.140]$	$[-0.490, 7.960]$
Isotropic Permittivity Range	$[0.00, 1.480]$	$[0.00, 1.480]$	$[0.00, 1.770]$	$[0.00, 2.190]$
Lens Curvature $l = 2.0$ [λ]				
	$s = 4.0$ [λ]	$s = 2.0$ [λ]	$s = 1.0$ [λ]	$s = 0.5$ [λ]
Anisotropic Permittivity Range	$[-0.180, 2.570]$	$[-0.310, 3.360]$	$[-0.490, 5.570]$	$[-0.730, 11.170]$
Isotropic Permittivity Range	$[0.00, 1.720]$	$[0.00, 1.790]$	$[0.00, 2.070]$	$[0.00, 2.590]$

Table II: Permittivity ranges of the physical lens.

1.1.3 Far-Field Patterns (Aniso-Lens, $\phi_s = 90.0$ [deg])

Lens Thickness $s = 4.0$ [λ]

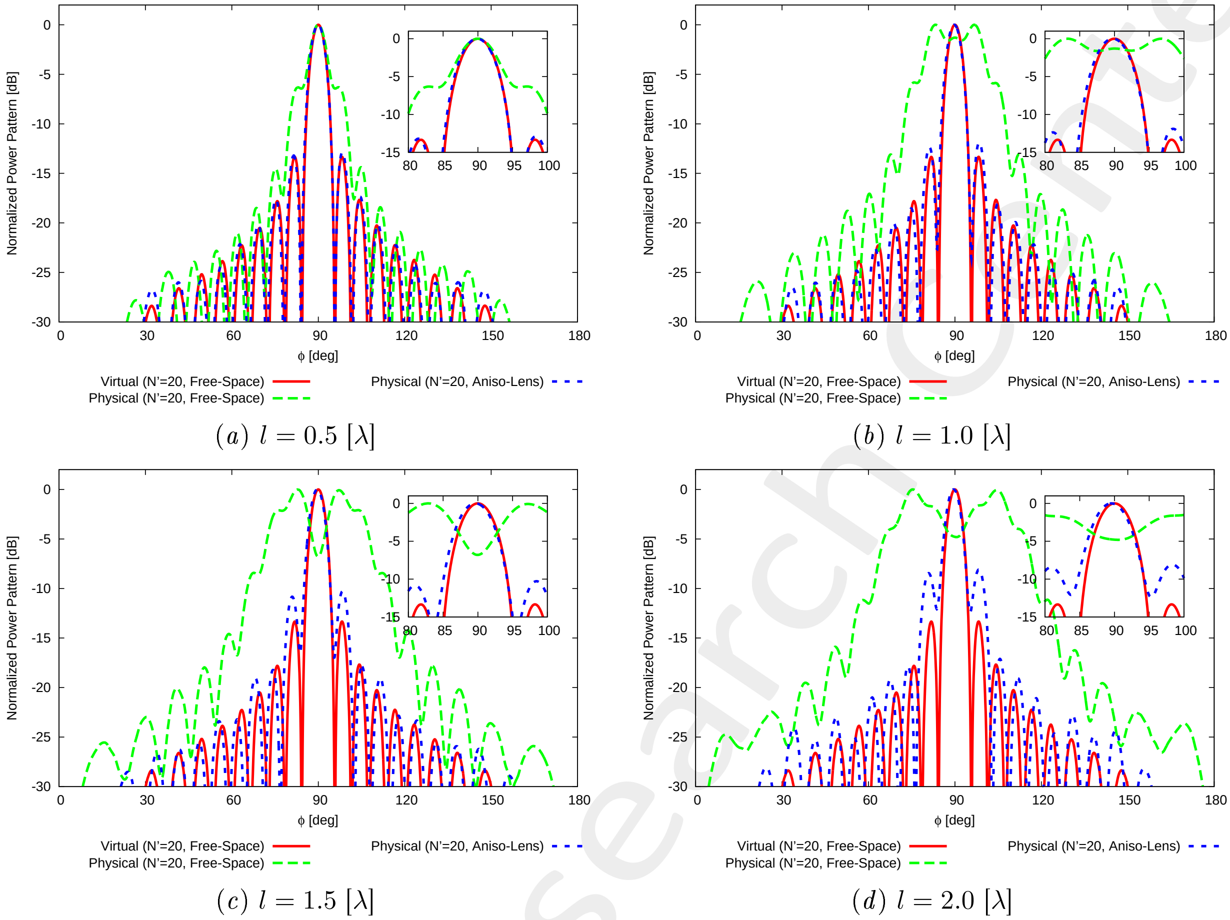

(a) $l = 0.5$ [λ]
(b) $l = 1.0$ [λ]
(c) $l = 1.5$ [λ]
(d) $l = 2.0$ [λ]

Figure 6: Lens thickness $s = 4.0$ [λ] - Comparison between the far field patterns or different curvatures of the lens.

Lens Thickness $s = 2.0$ $[\lambda]$

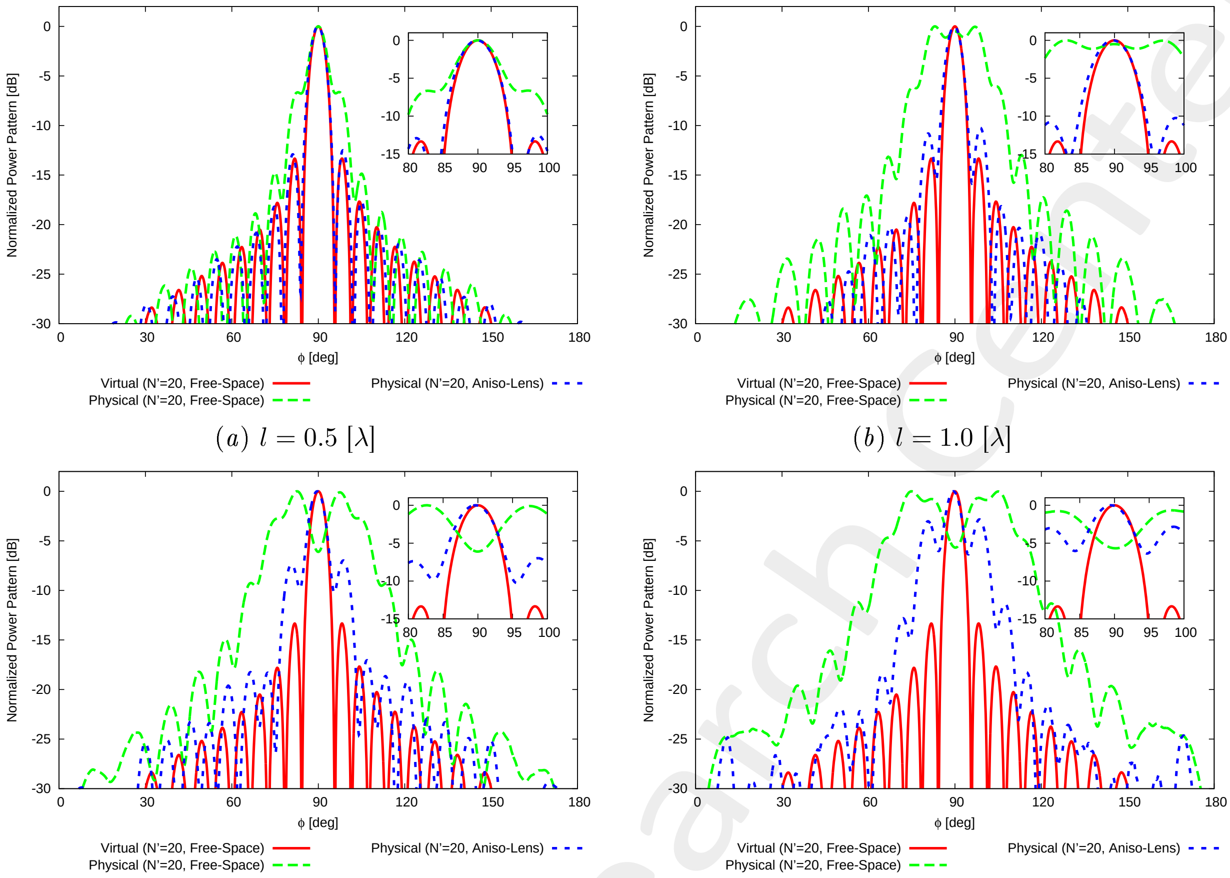

(a) $l = 0.5$ $[\lambda]$ (b) $l = 1.0$ $[\lambda]$

(c) $l = 1.5$ $[\lambda]$ (d) $l = 2.0$ $[\lambda]$

Figure 7: Lens thickness $s = 2.0$ $[\lambda]$ - Comparison between the far field patterns or different curvatures of the lens.

Lens Thickness $s = 1.0$ [λ]

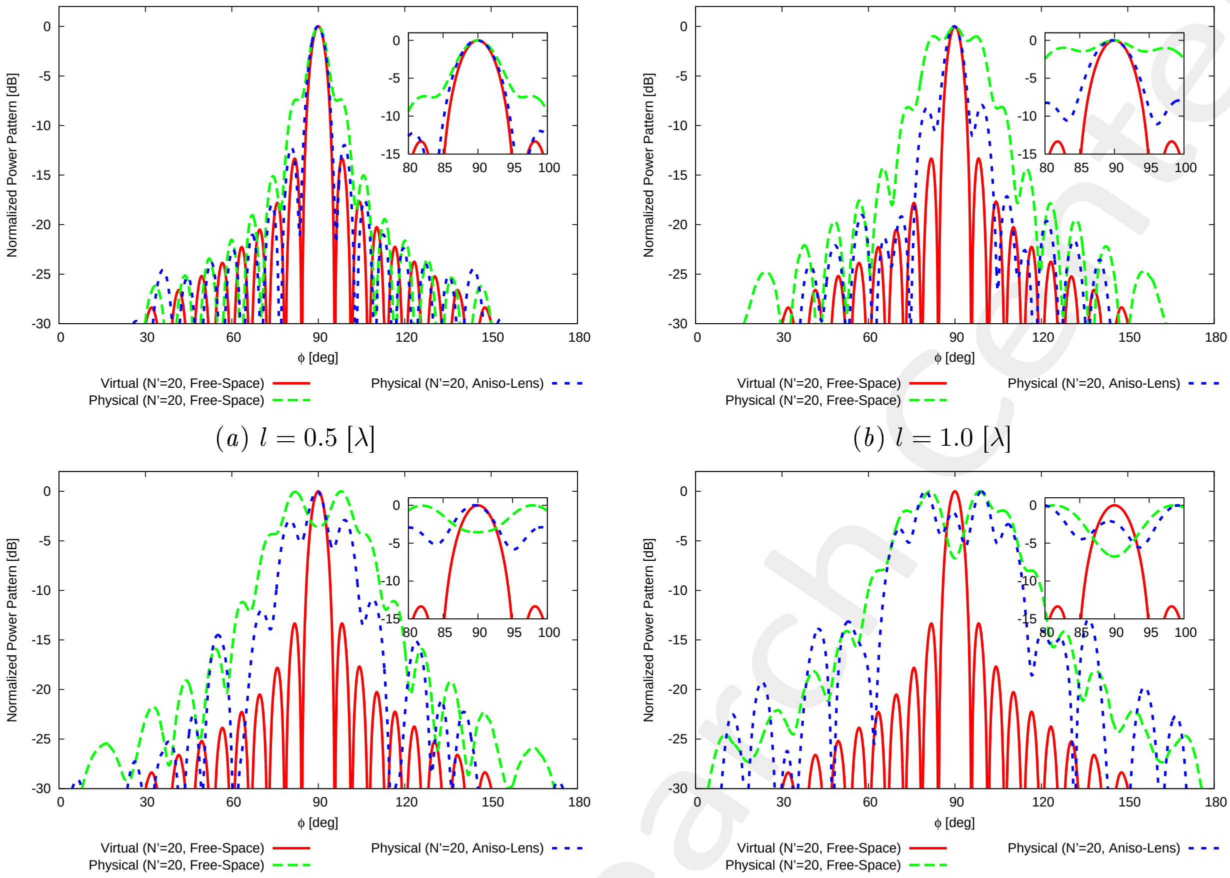

(a) $l = 0.5$ [λ] (b) $l = 1.0$ [λ]

(c) $l = 1.5$ [λ] (d) $l = 2.0$ [λ]

Figure 8: Lens thickness $s = 1.0$ [λ] - Comparison between the far field patterns or different curvatures of the lens.

Lens Thickness $s = 0.5$ [λ]

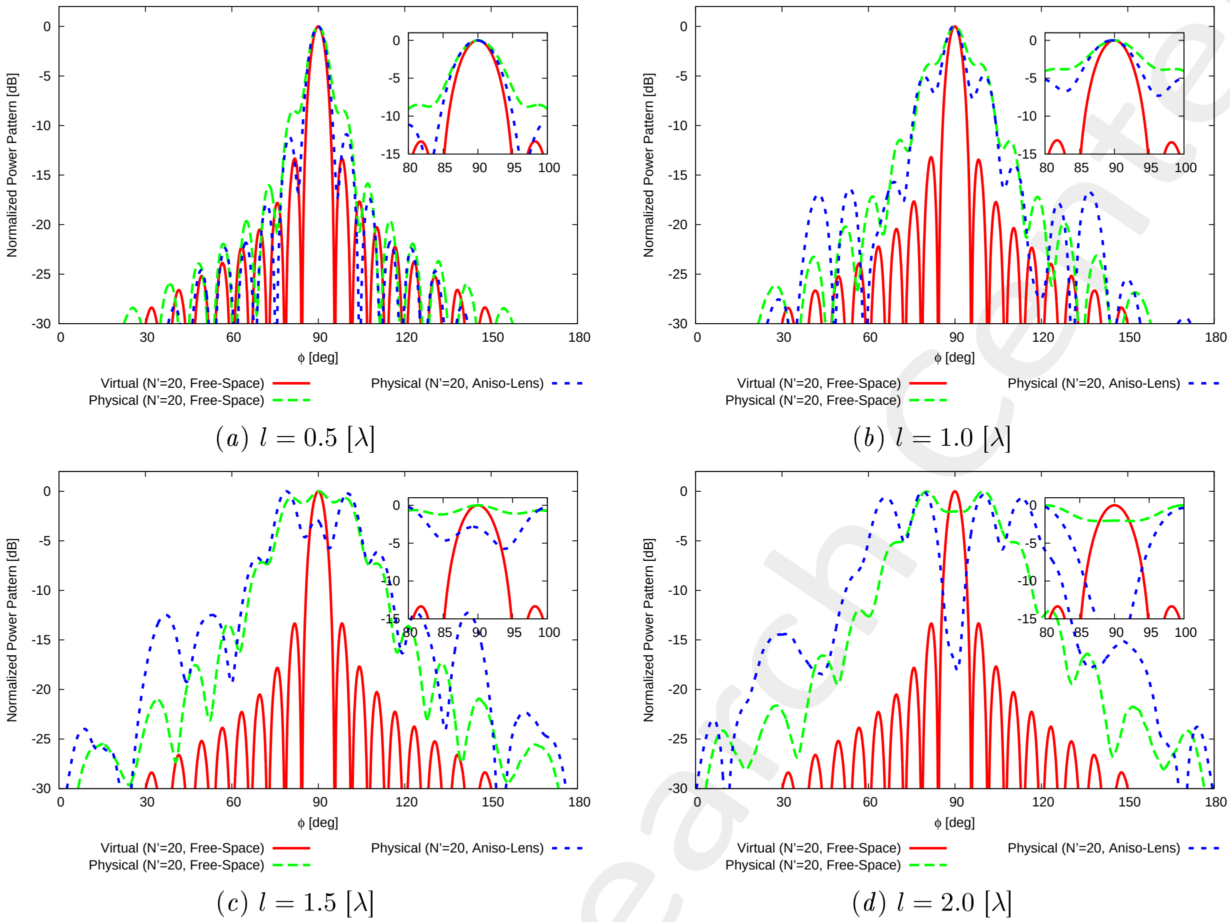

Figure 9: Lens thickness $s = 0.5$ [λ] - Comparison between the far field patterns or different curvatures of the lens.

Observations

- Increasing the curvature ($\uparrow l$) leads to a worsening of the performances;
- Decreasing the lens thickness ($\downarrow s$) leads to a worsening of the performances;
- The thinner the lens, the fastest the degradation w.r.t. the curvature.

1.2 Lens Thickness $s = 4.0$ [λ] - Reduction of the Control Points through SI ($N' \rightarrow N < N'$)

Parameters

- Number of array elements before SI: $N' = 20$;
- Number of array elements after SI (N): check table below;
- Spacing after SI: $d = \lambda/2$;
- Radius of the observation domain: $r_{SI} = 50.0$ [λ];
- Number of field sampling points: $n_{SI} = 1000$.

	Before SI		**After SI**	
l [λ] (Lens Curvature)	N'	L [λ]	N	L [λ]
0.5	20	9.042	19	9.0
1.0	20	8.670	18	8.5
1.5	20	8.340	18	8.5
2.0	20	8.090	17	8.0

Table III: Lens Thickness $s = 4.0$ [λ] - Parameters considered for SI for each curvature of the physical lens (l).

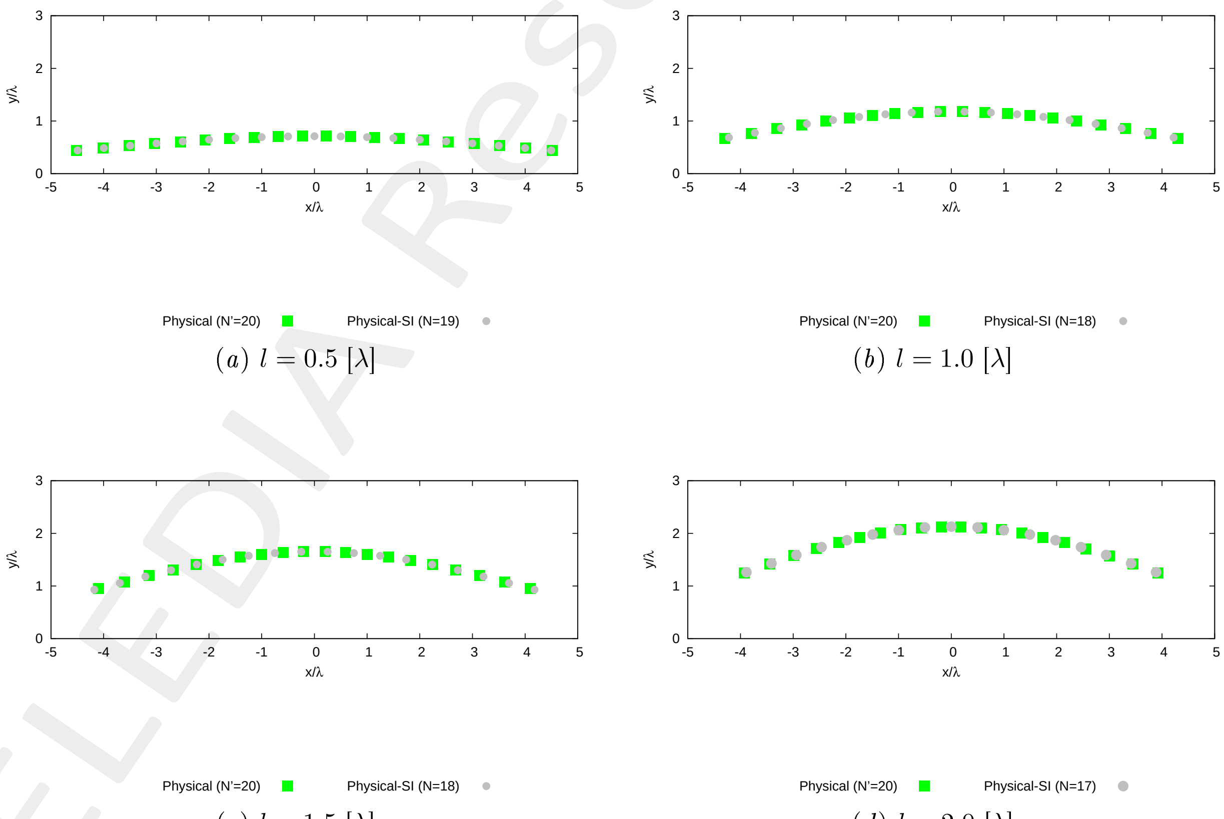

(a) $l = 0.5$ [λ] (b) $l = 1.0$ [λ] (c) $l = 1.5$ [λ] (d) $l = 2.0$ [λ]

Figure 10: Lens Thickness $s = 4.0$ [λ] - Geometry of the physical array before (N') and after SI ($N < N'$).

1.2.1 Synthesized Excitations

Steering Angle $\phi_s = 90.0$ [deg]

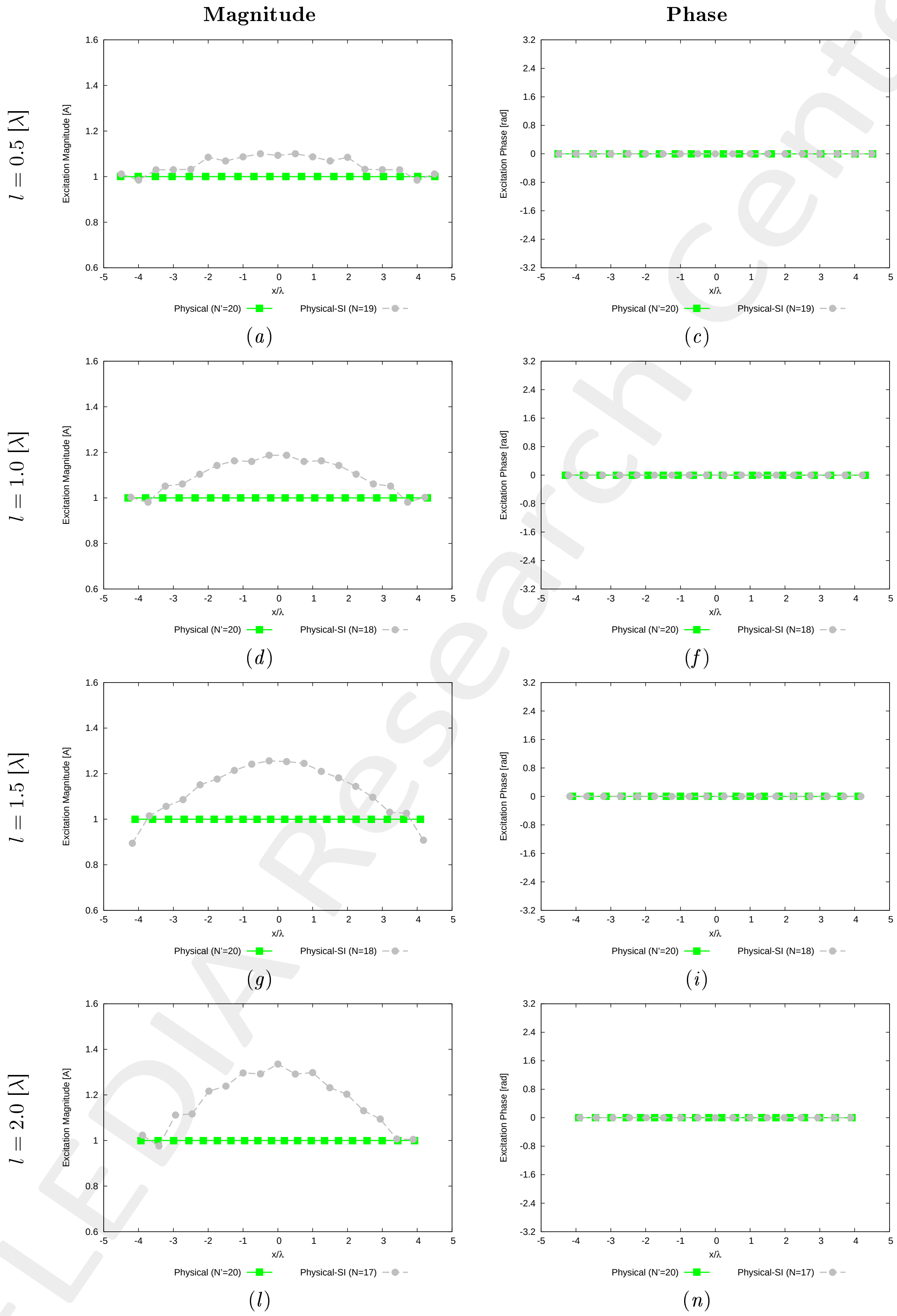

Figure 11: Lens Thickness $s = 4.0$ [λ] - Magnitude and phase of the excitations of the physical array before (N') and after SI ($N < N'$).

Steering Angle $\phi_s = 75.0$ [deg]

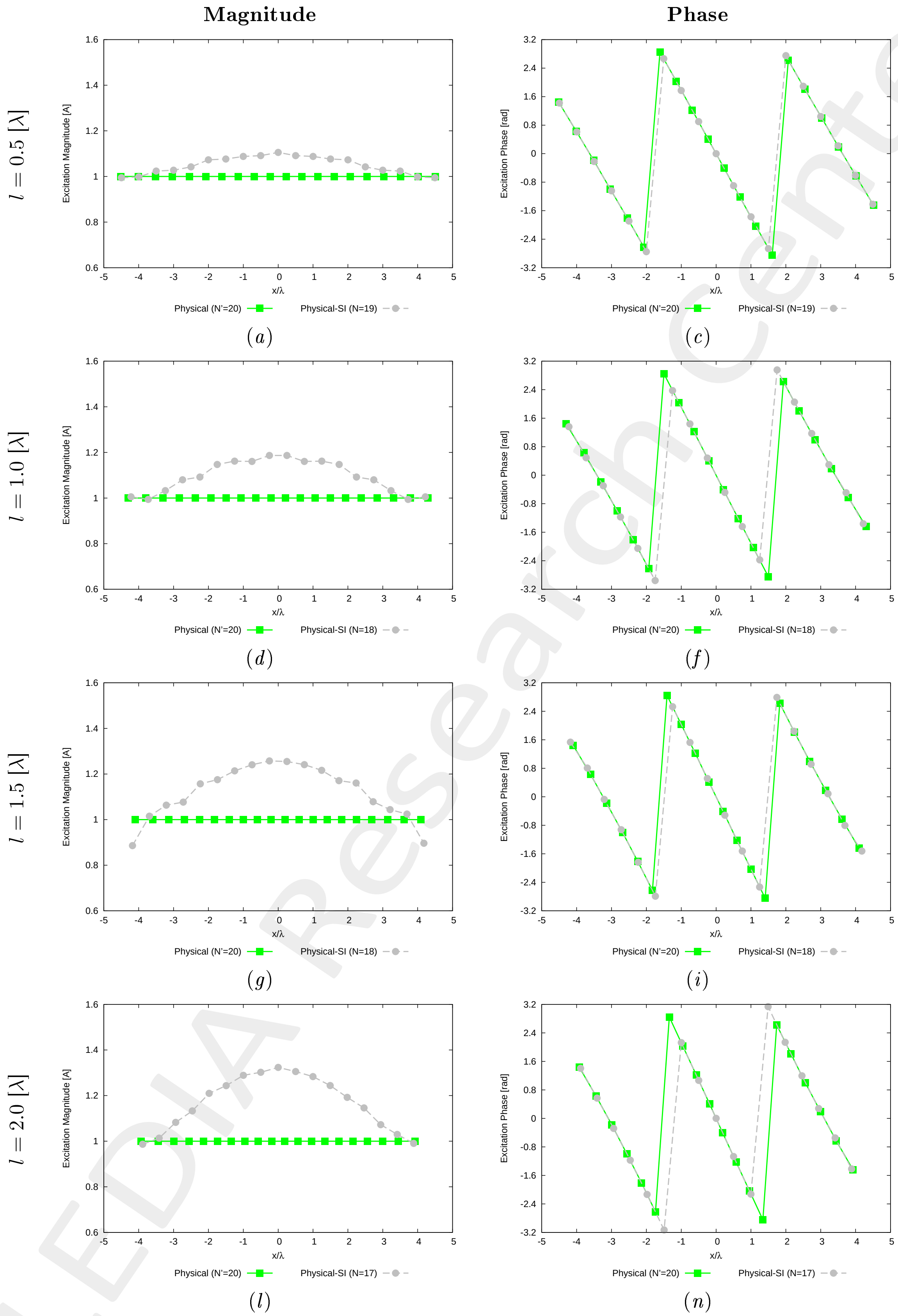

Figure 12: Lens Thickness $s = 4.0$ [λ] - Magnitude and phase of the excitations of the physical array before (N') and after SI ($N < N'$).

Steering Angle $\phi_s = 60.0$ **[**deg**]**

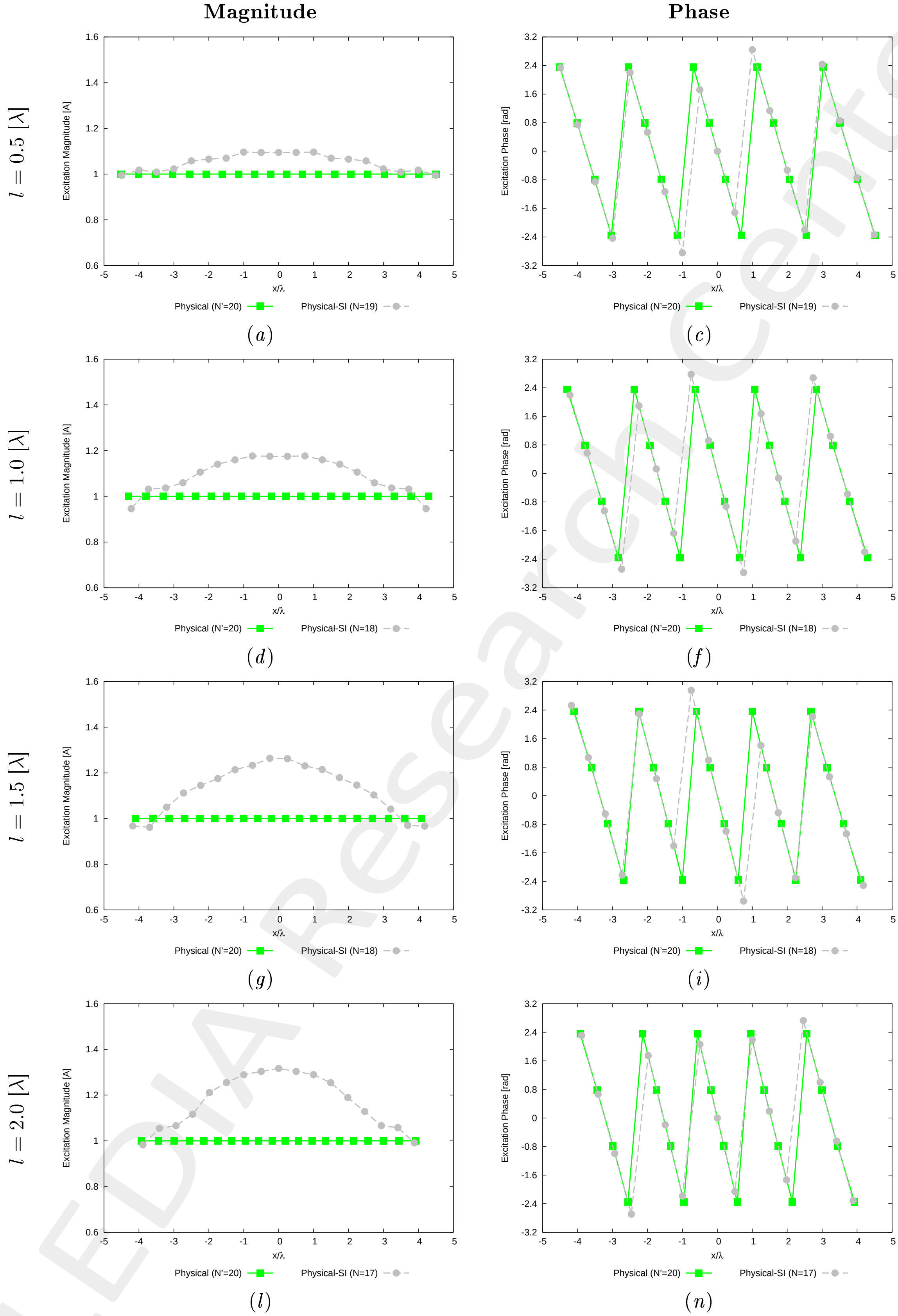

Figure 13: Lens Thickness $s = 4.0$ [λ] - Magnitude and phase of the excitations of the physical array before (N') and after SI ($N < N'$).

Steering Angle $\phi_s = 45.0$ $[deg]$

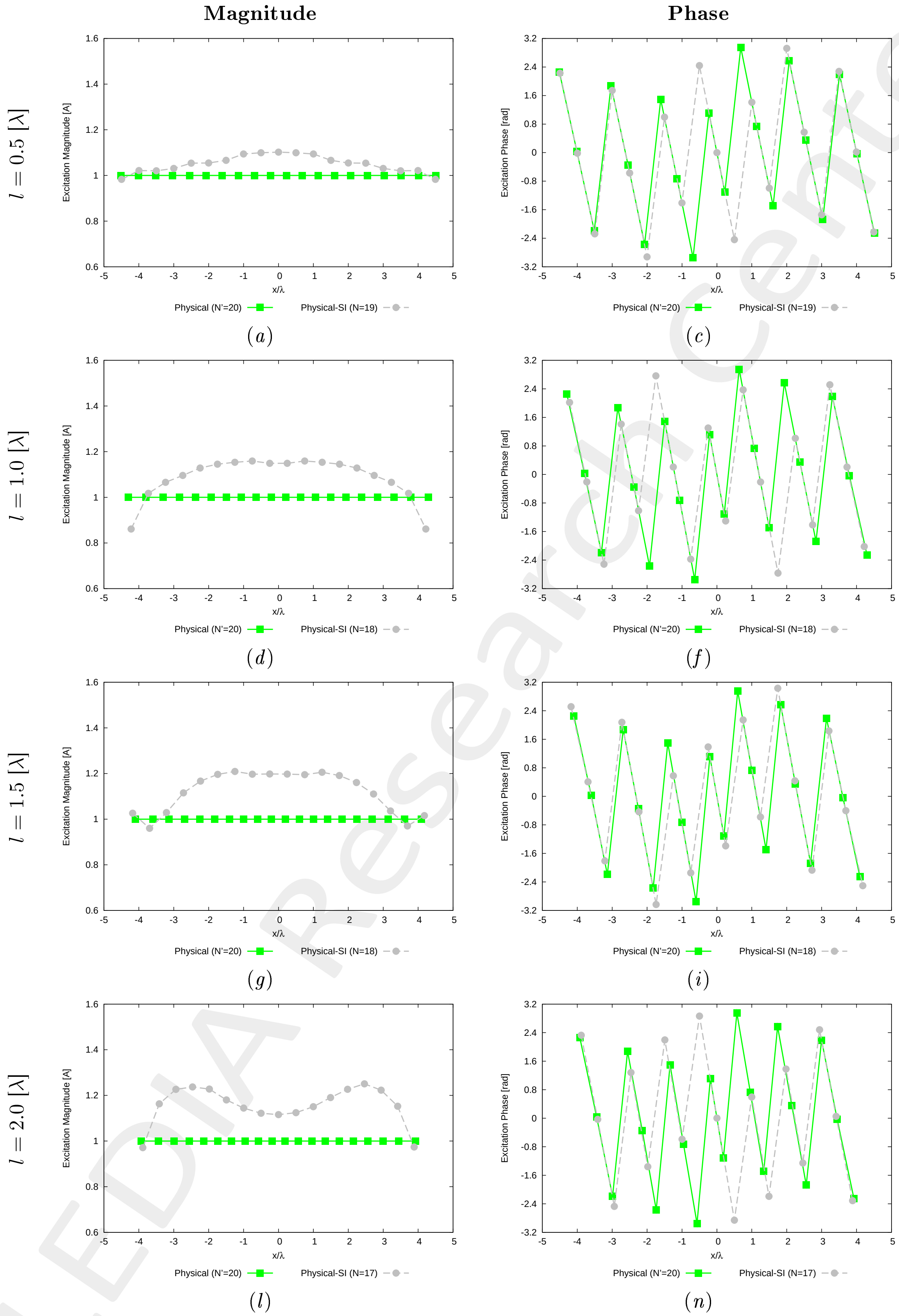

Figure 14: Lens Thickness $s = 4.0$ $[\lambda]$ - Magnitude and phase of the excitations of the physical array before (N') and after SI $(N < N')$.

1.2.2 Free-Space Far-Field Patterns (check SI)

Steering Angle $\phi_s = 90.0$ **[**deg**]**

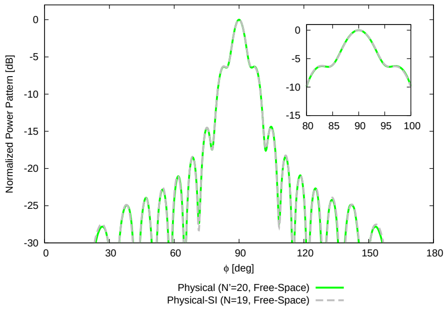

(a) $l = 0.5$ $[\lambda]$

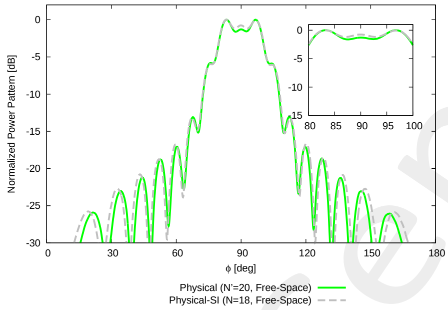

(b) $l = 1.0$ $[\lambda]$

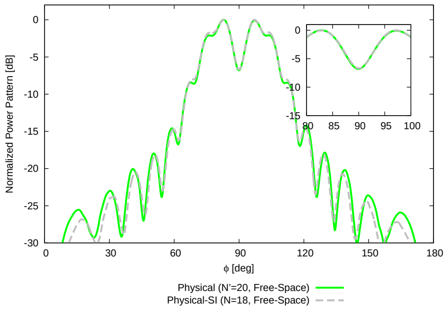

(c) $l = 1.5$ $[\lambda]$

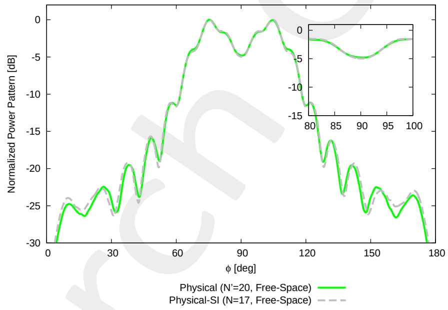

(d) $l = 2.0$ $[\lambda]$

Figure 15: Lens Thickness $s = 4.0$ $[\lambda]$ - Free-Space patterns: Physical ($N' = 20$) vs. Physical-SI ($N < N'$).

Steering Angle $\phi_s = 75.0$ **[**deg**]**

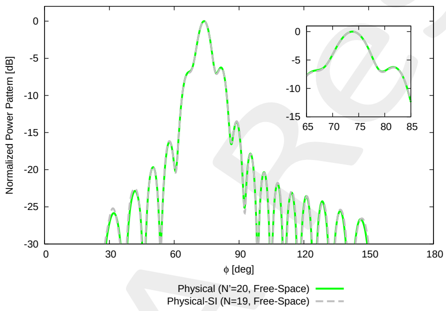

(a) $l = 0.5$ $[\lambda]$

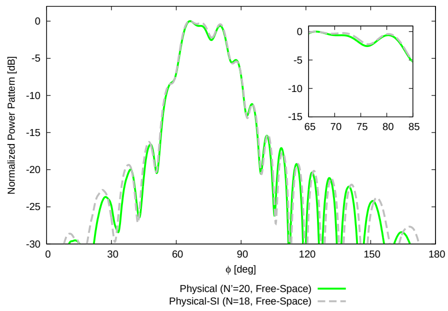

(b) $l = 1.0$ $[\lambda]$

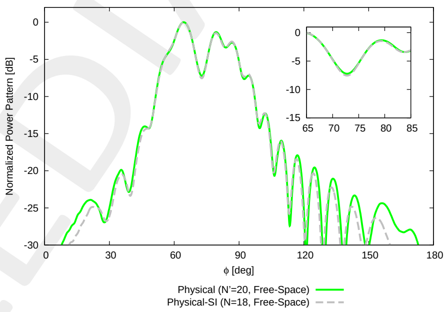

(c) $l = 1.5$ $[\lambda]$

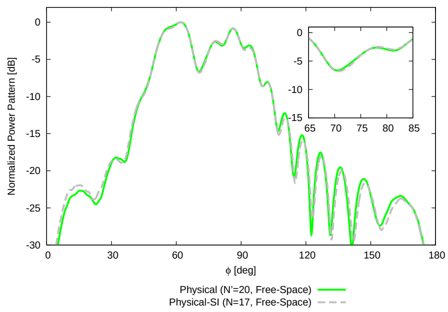

(d) $l = 2.0$ $[\lambda]$

Figure 16: Lens Thickness $s = 4.0$ $[\lambda]$ - Free-Space patterns: Physical ($N' = 20$) vs. Physical-SI ($N < N'$).

Steering Angle $\phi_s = 60.0$ [deg]

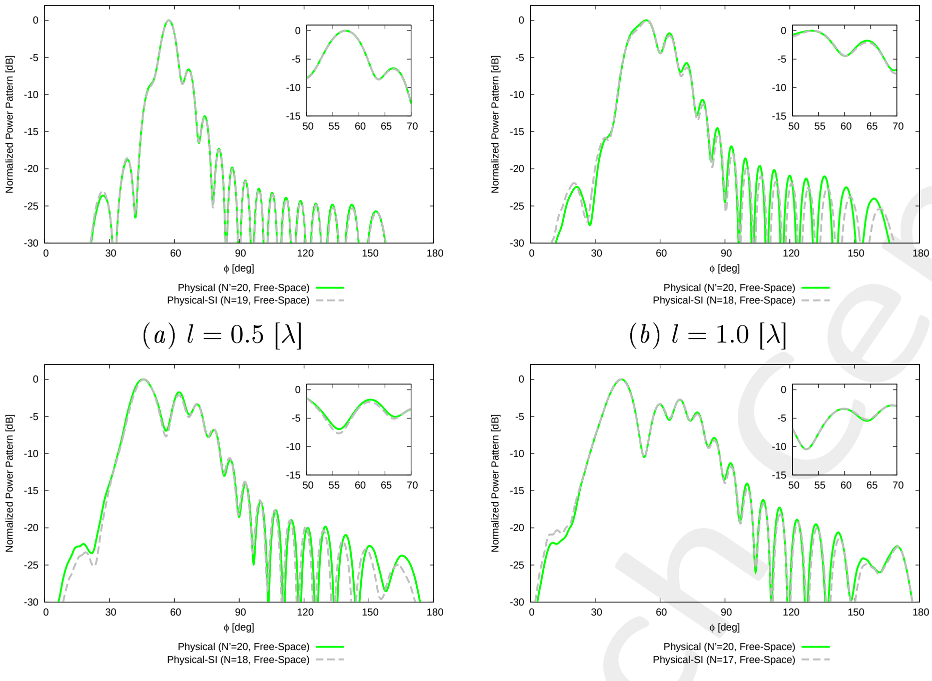

(a) $l = 0.5$ [λ] (b) $l = 1.0$ [λ]

(c) $l = 1.5$ [λ] (d) $l = 2.0$ [λ]

Figure 17: Lens Thickness $s = 4.0$ [λ] - Free-Space patterns: Physical ($N' = 20$) vs. Physical-SI ($N < N'$).

Steering Angle $\phi_s = 45.0$ [deg]

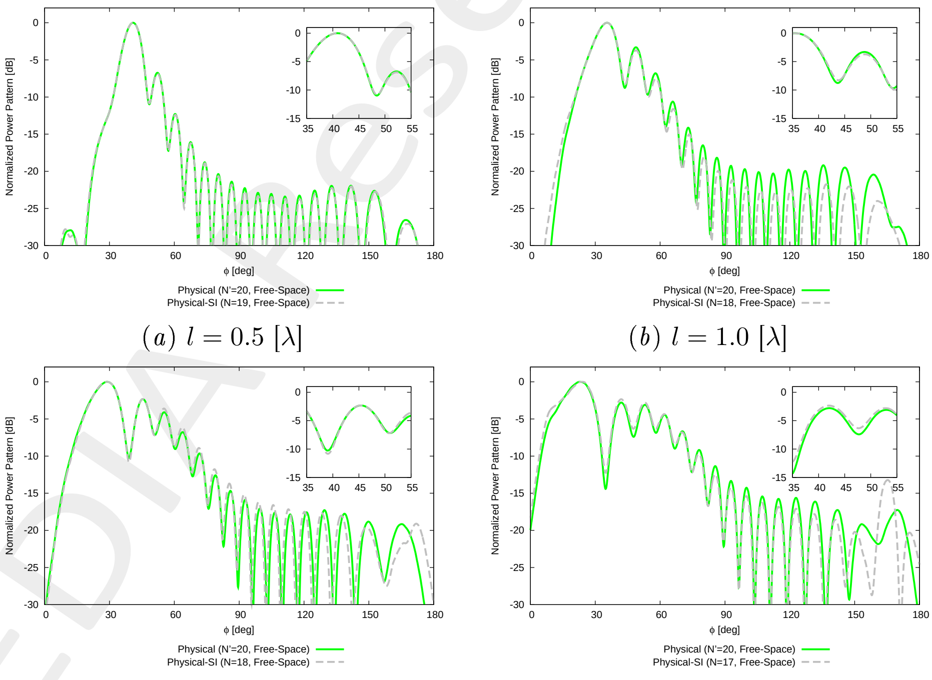

(a) $l = 0.5$ [λ] (b) $l = 1.0$ [λ]

(c) $l = 1.5$ [λ] (d) $l = 2.0$ [λ]

Figure 18: Lens Thickness $s = 4.0$ [λ] - Free-Space patterns: Physical ($N' = 20$) vs. Physical-SI ($N < N'$).

1.2.3 Near-Field Distributions (Aniso-Lens, $\phi_s = 90.0$ [deg])

Curvature $l = 0.5$ [λ]

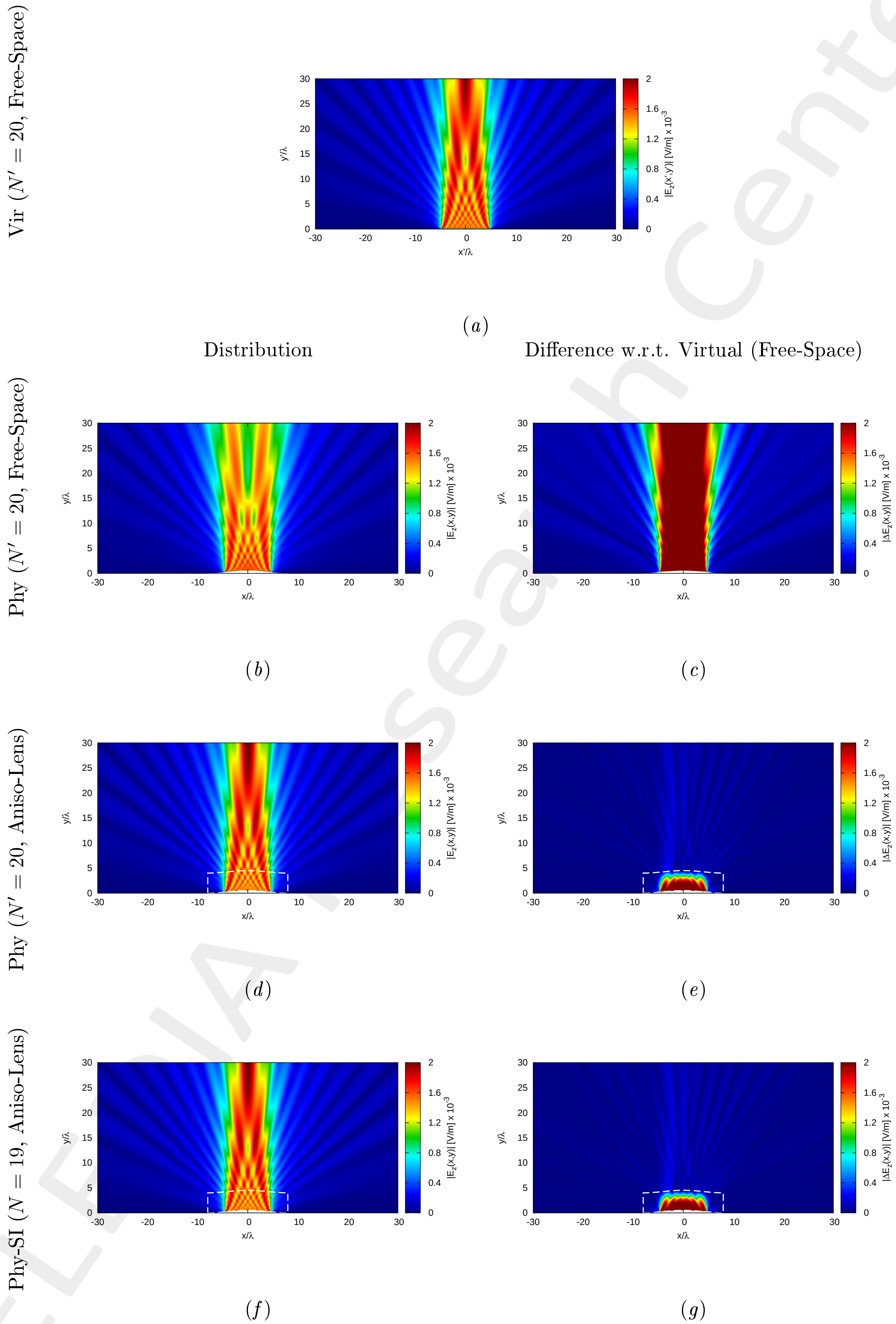

Figure 19: Lens Thickness $s = 4.0$ [λ] - Electric field distributions.

Curvature $l = 1.0$ [λ]

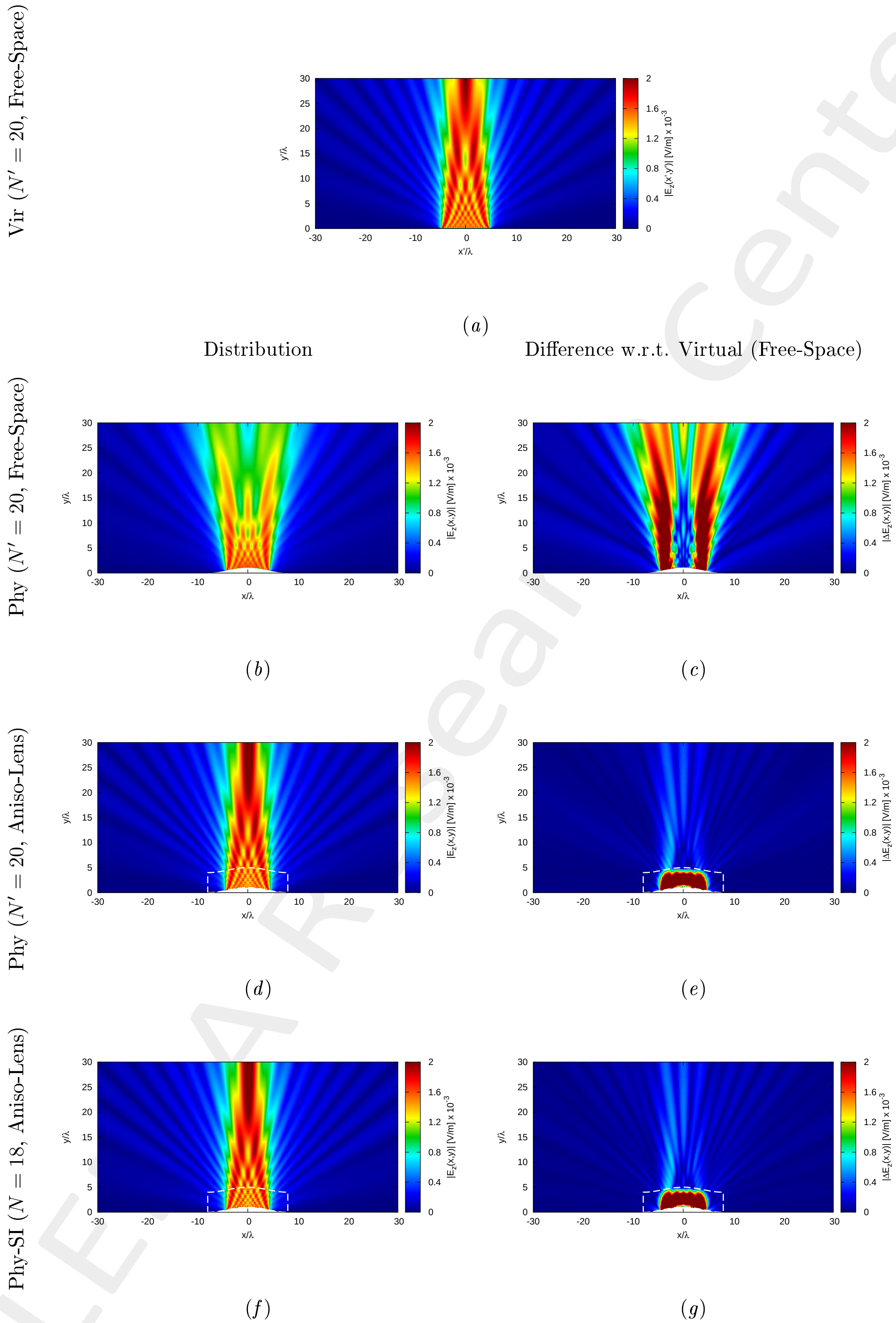

Figure 20: Lens Thickness $s = 4.0$ [λ] - Electric field distributions.

Curvature $l = 1.5$ $[\lambda]$

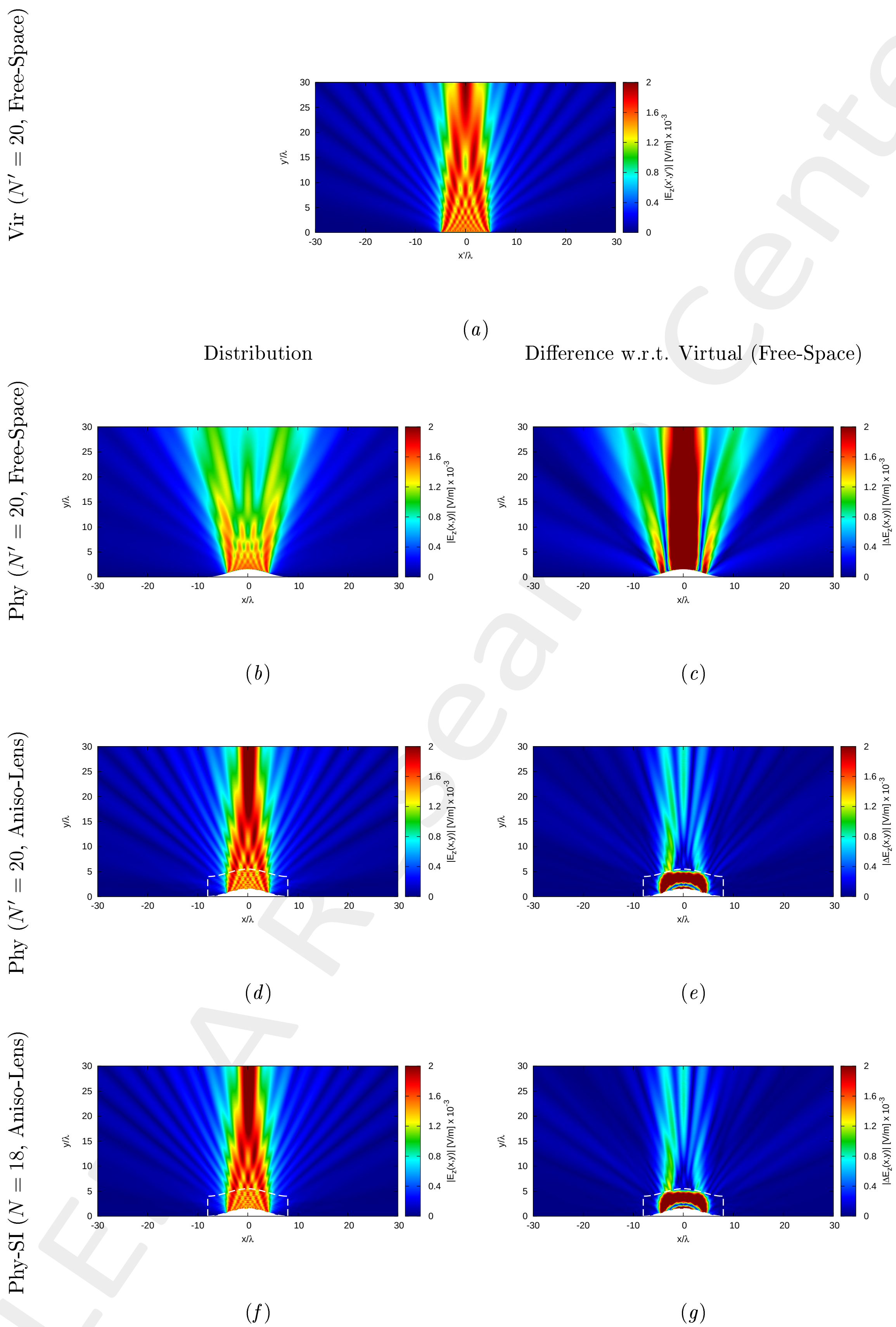

Figure 21: Lens Thickness $s = 4.0$ $[\lambda]$ - Electric field distributions.

Curvature $l = 2.0$ [λ]

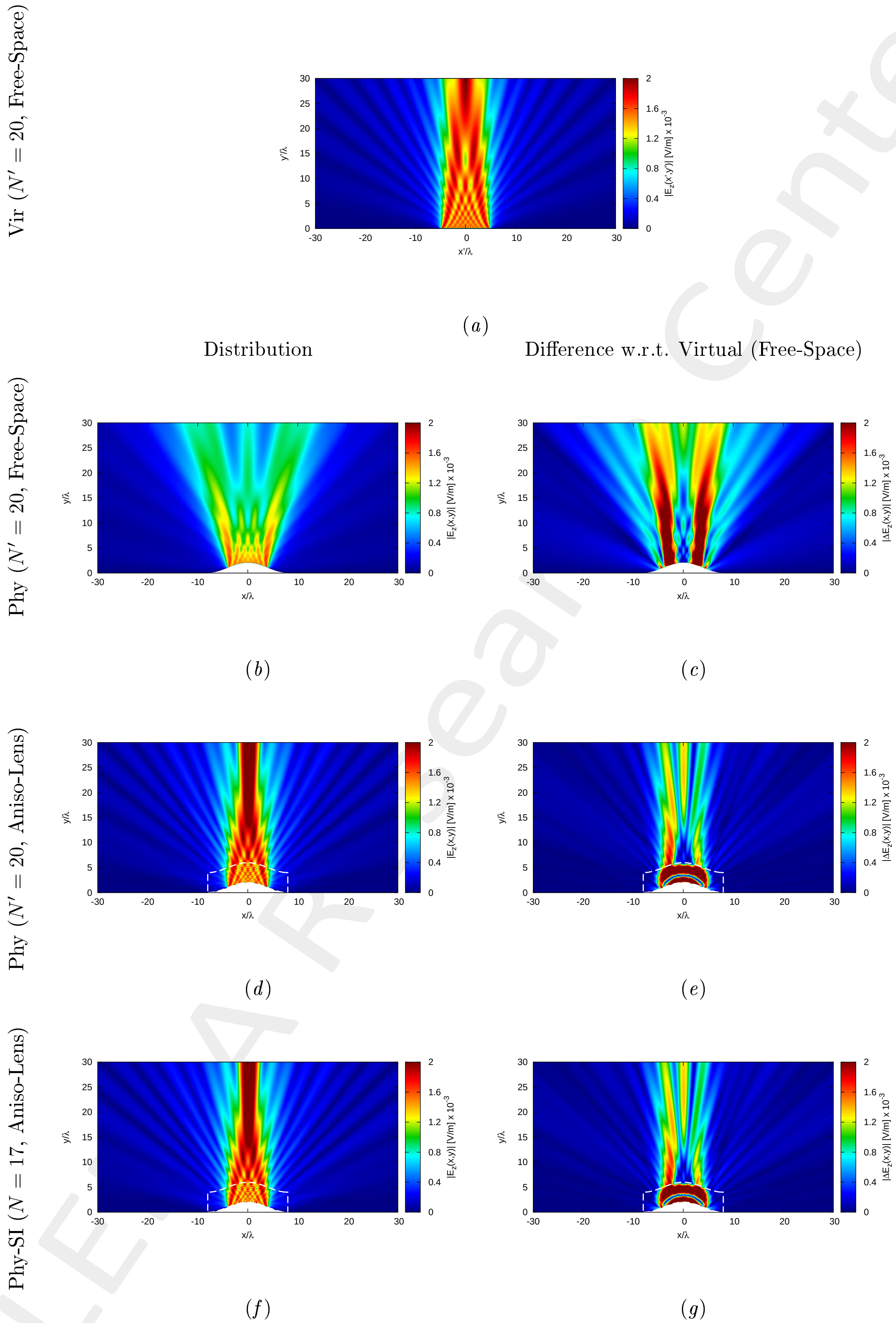

Figure 22: Lens Thickness $s = 4.0$ [λ] - Electric field distributions.

1.2.4 Near-Field Distributions (Aniso-Lens, $\phi_s = 75.0$ [deg])

Curvature $l = 0.5$ [λ]

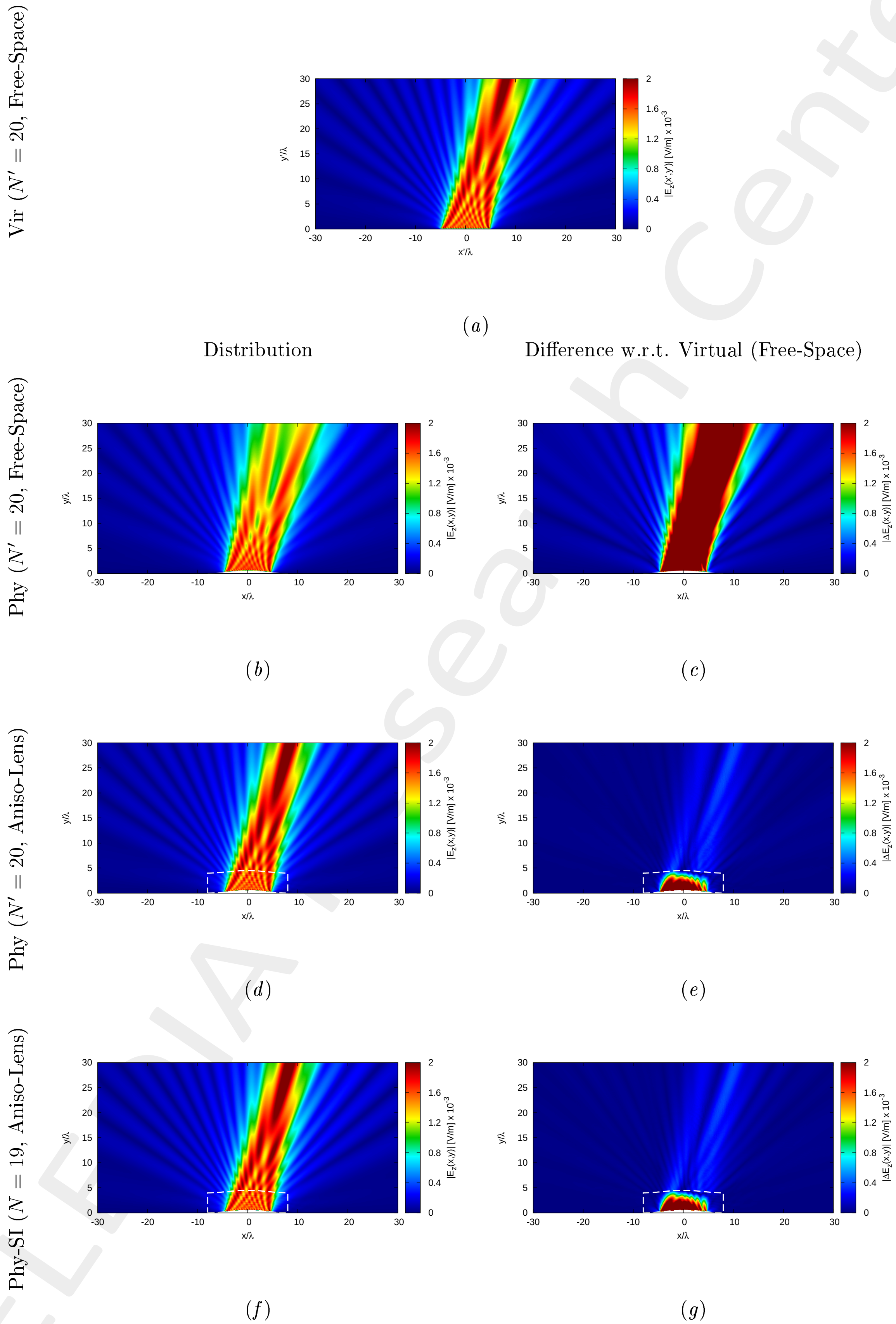

Figure 23: Lens Thickness $s = 4.0$ [λ] - Electric field distributions.

Curvature $l = 1.0$ $[\lambda]$

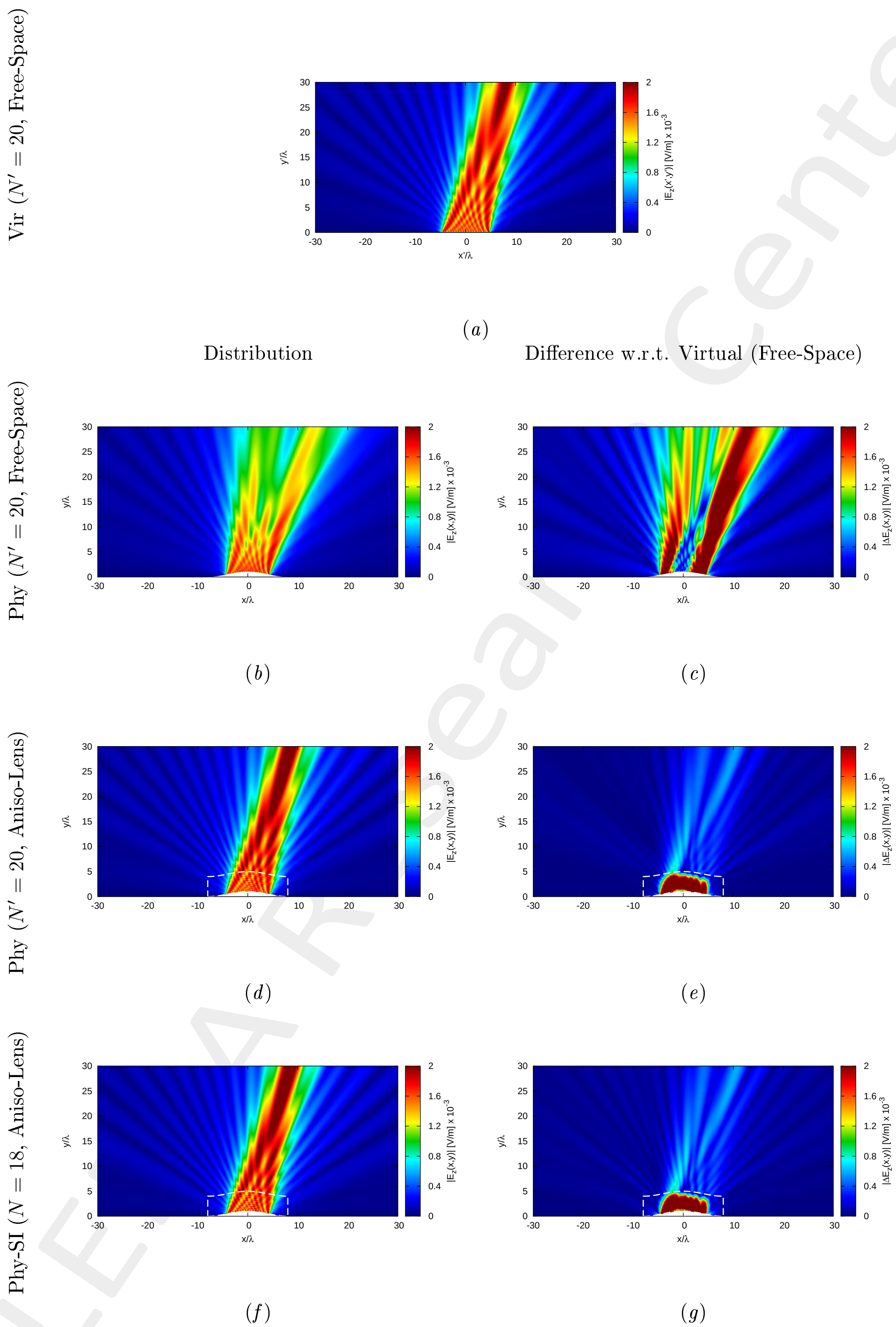

Figure 24: Lens Thickness $s = 4.0$ $[\lambda]$ - Electric field distributions.

Curvature $l = 1.5$ $[\lambda]$

Vir ($N' = 20$, Free-Space)

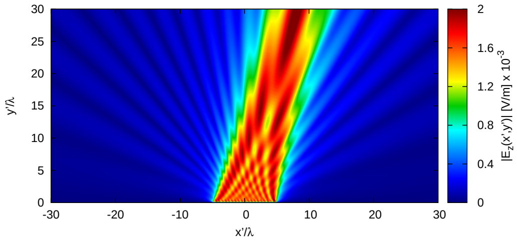

(a)

Distribution

Difference w.r.t. Virtual (Free-Space)

Phy ($N' = 20$, Free-Space)

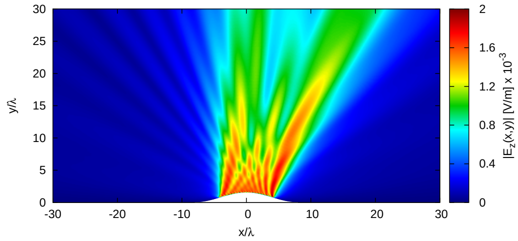

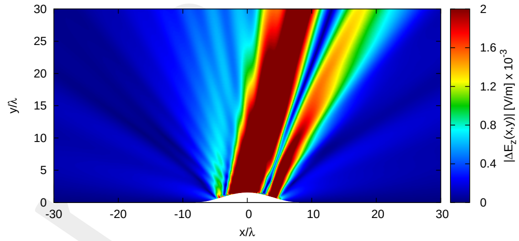

(b) (c)

Phy ($N' = 20$, Aniso-Lens)

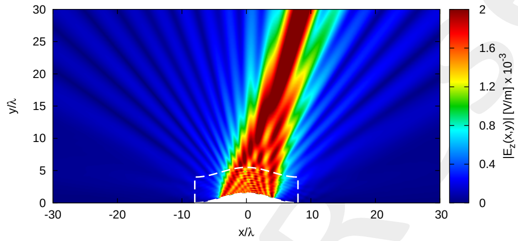

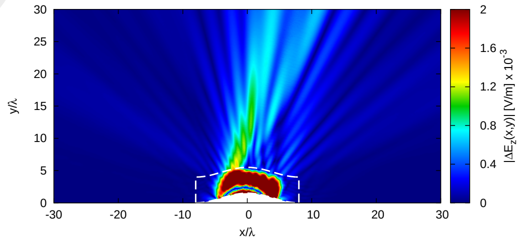

(d) (e)

Phy-SI ($N = 18$, Aniso-Lens)

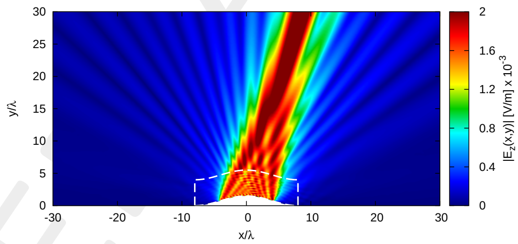

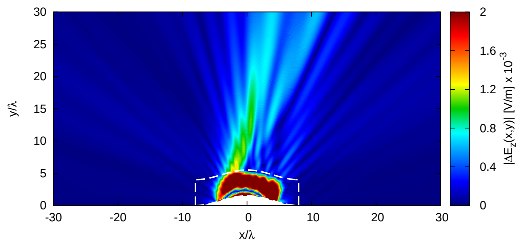

(f) (g)

Figure 25: Lens Thickness $s = 4.0$ $[\lambda]$ - Electric field distributions.

Curvature $l = 2.0$ $[\lambda]$

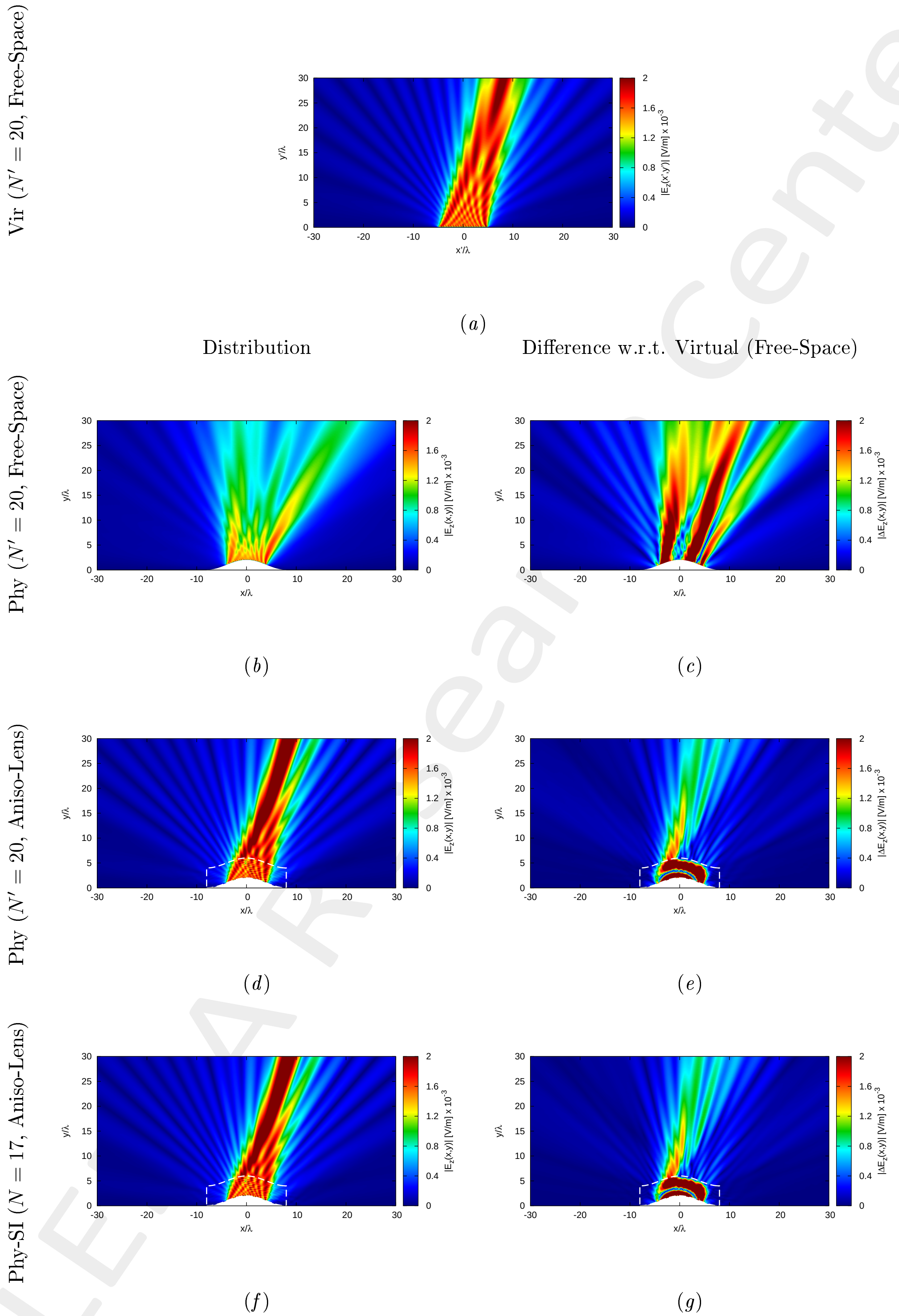

Figure 26: Lens Thickness $s = 4.0$ $[\lambda]$ - Electric field distributions.

1.2.5 Near-Field Distributions (Aniso-Lens, $\phi_s = 60.0$ [deg])

Curvature $l = 0.5$ [λ]

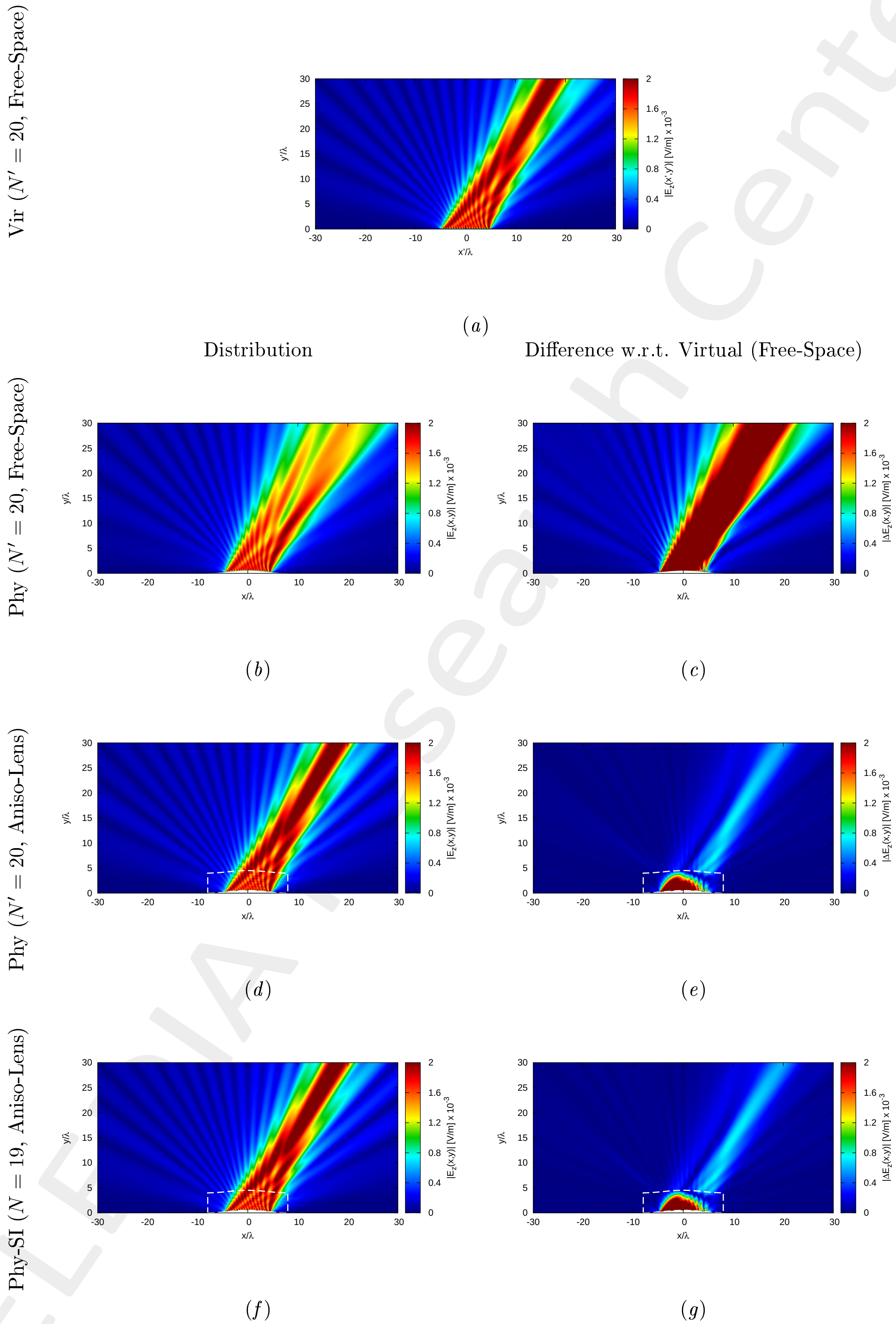

Figure 27: Lens Thickness $s = 4.0$ [λ] - Electric field distributions.

Curvature $l = 1.0$ [λ]

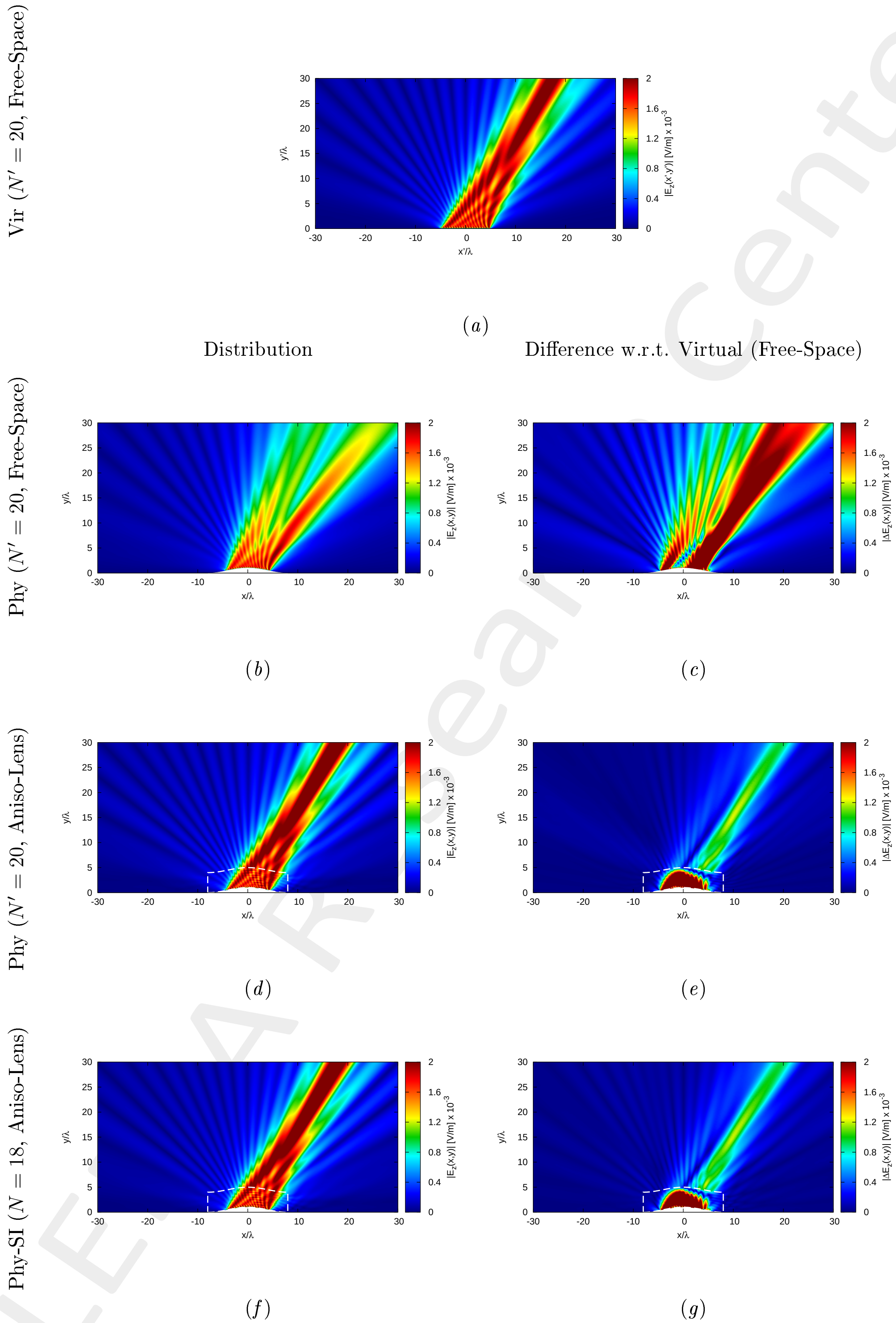

Figure 28: Lens Thickness $s = 4.0$ [λ] - Electric field distributions.

Curvature $l = 1.5$ [λ]

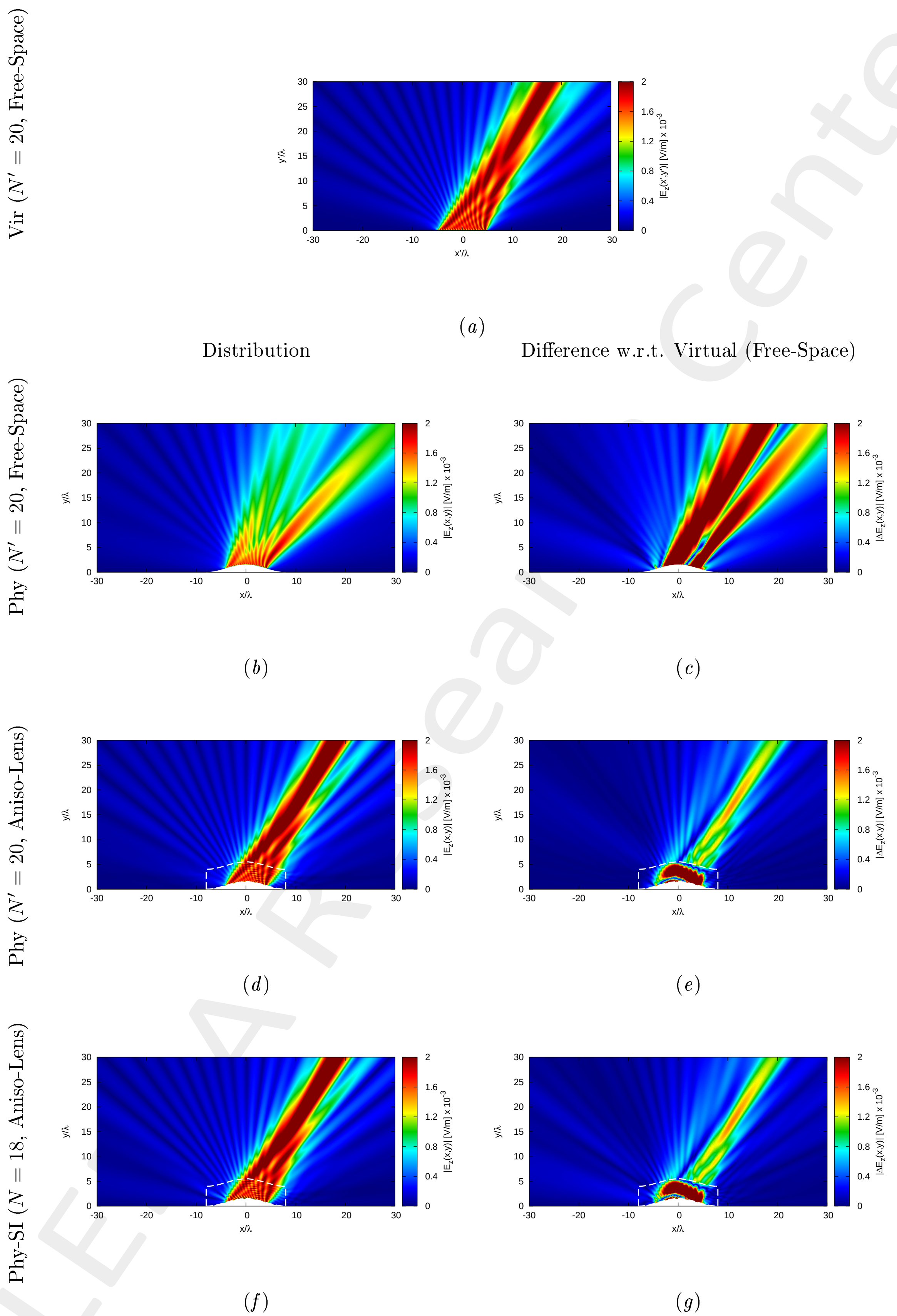

Figure 29: Lens Thickness $s = 4.0$ [λ] - Electric field distributions.

Curvature $l = 2.0$ $[\lambda]$

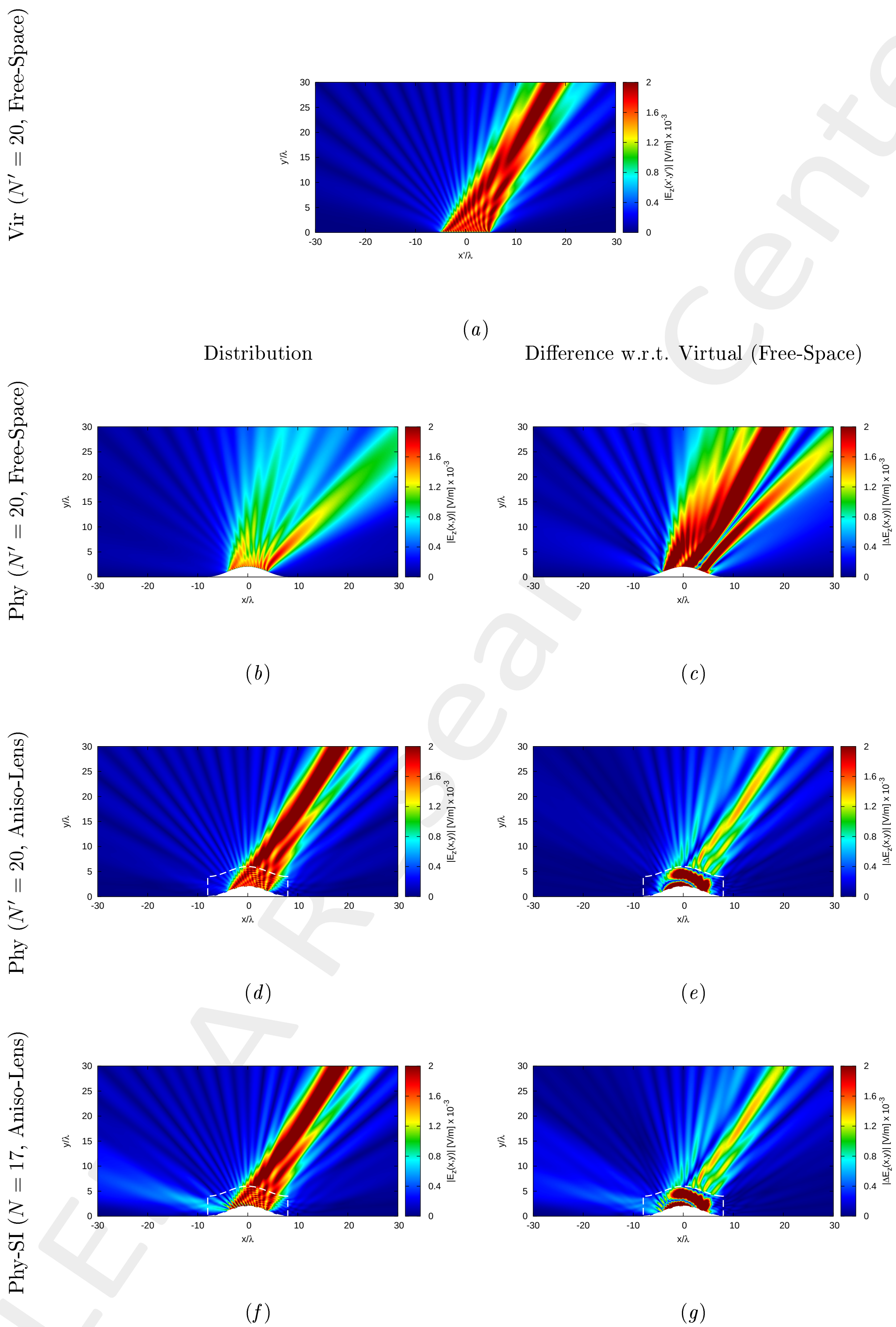

Figure 30: Lens Thickness $s = 4.0$ $[\lambda]$ - Electric field distributions.

1.2.6 Near-Field Distributions (Aniso-Lens, $\phi_s = 45.0$ [deg])

Curvature $l = 0.5$ [λ]

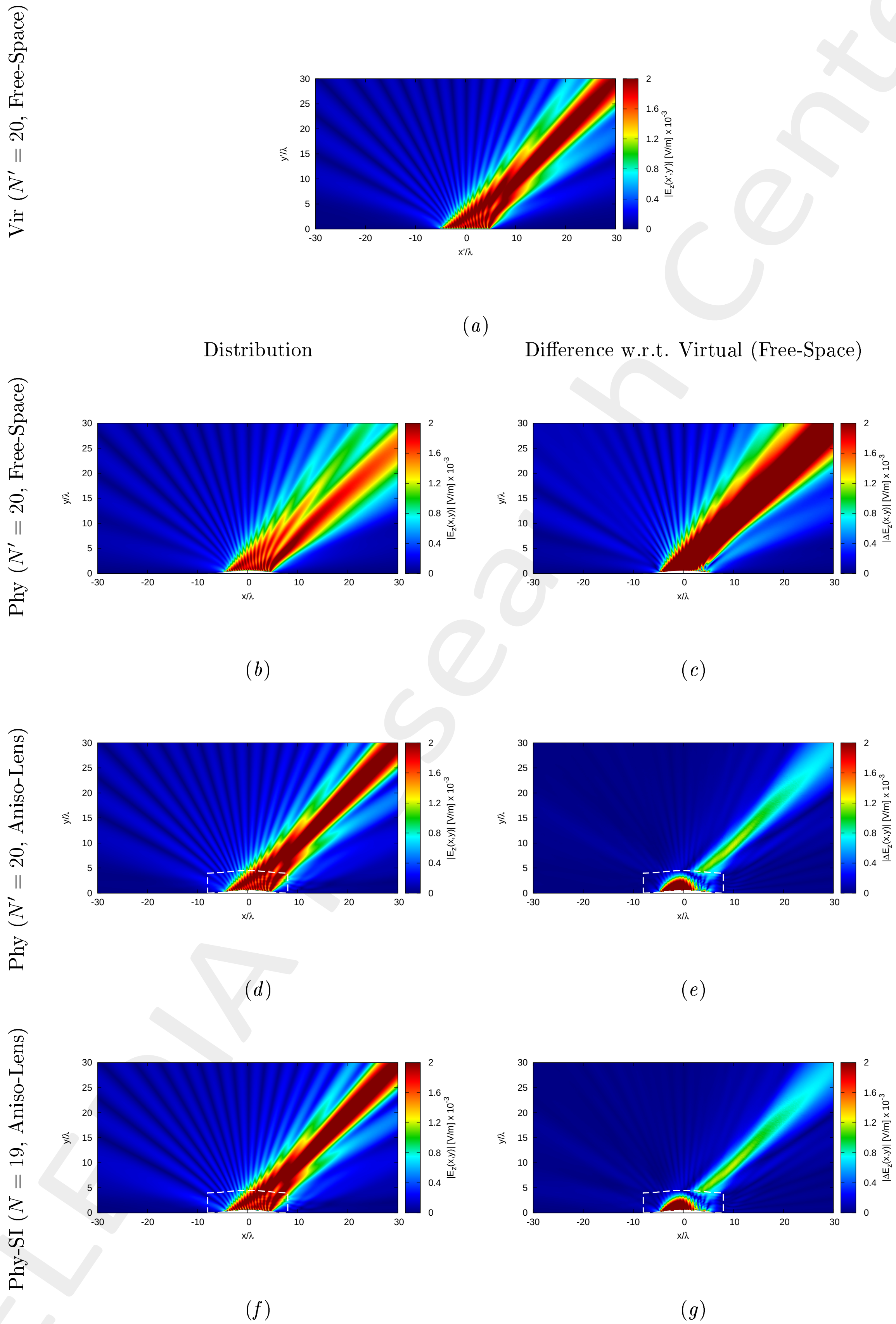

Figure 31: Lens Thickness $s = 4.0$ [λ] - Electric field distributions.

Curvature $l = 1.0$ $[\lambda]$

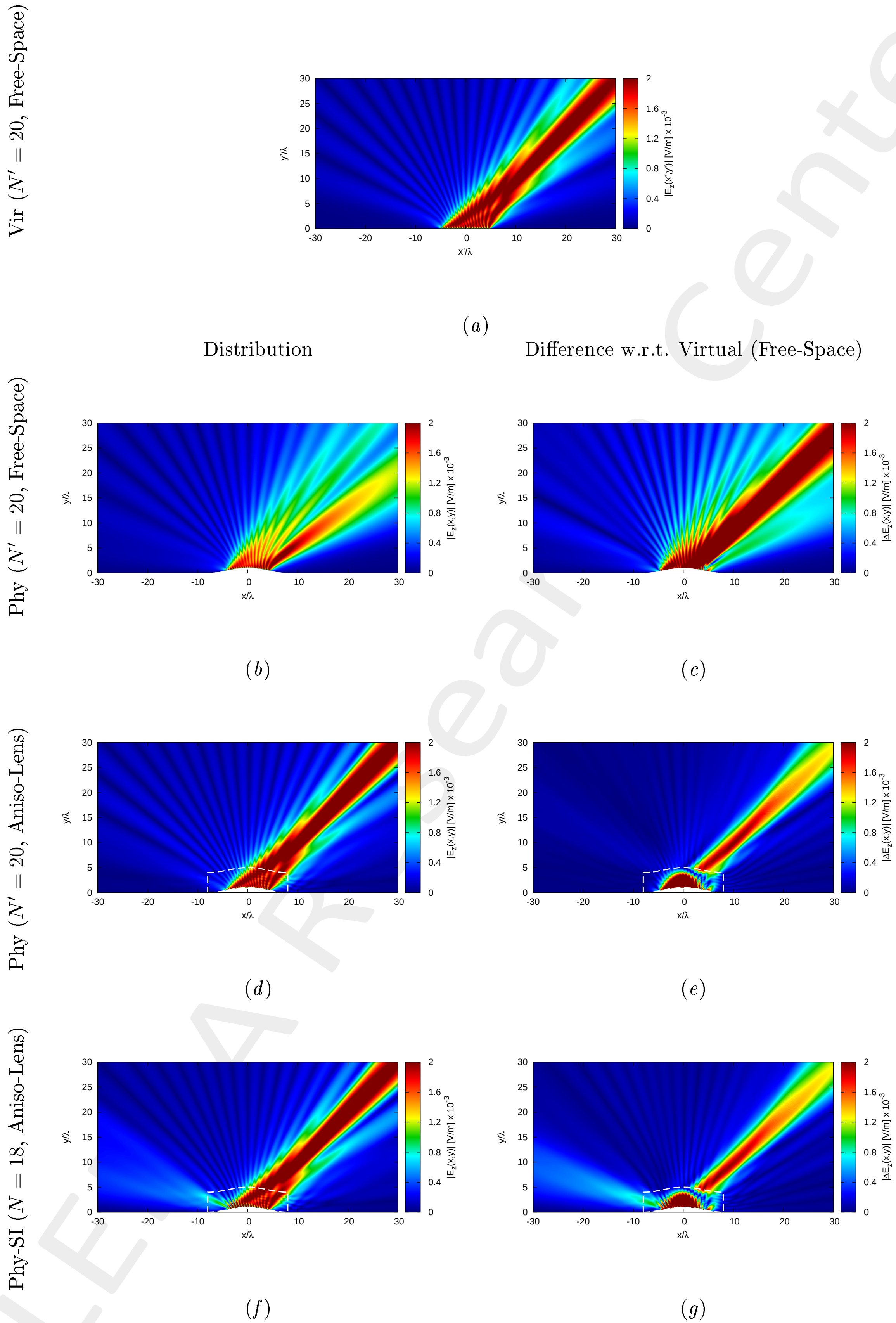

Figure 32: Lens Thickness $s = 4.0$ $[\lambda]$ - Electric field distributions.

Curvature $l = 1.5$ $[\lambda]$

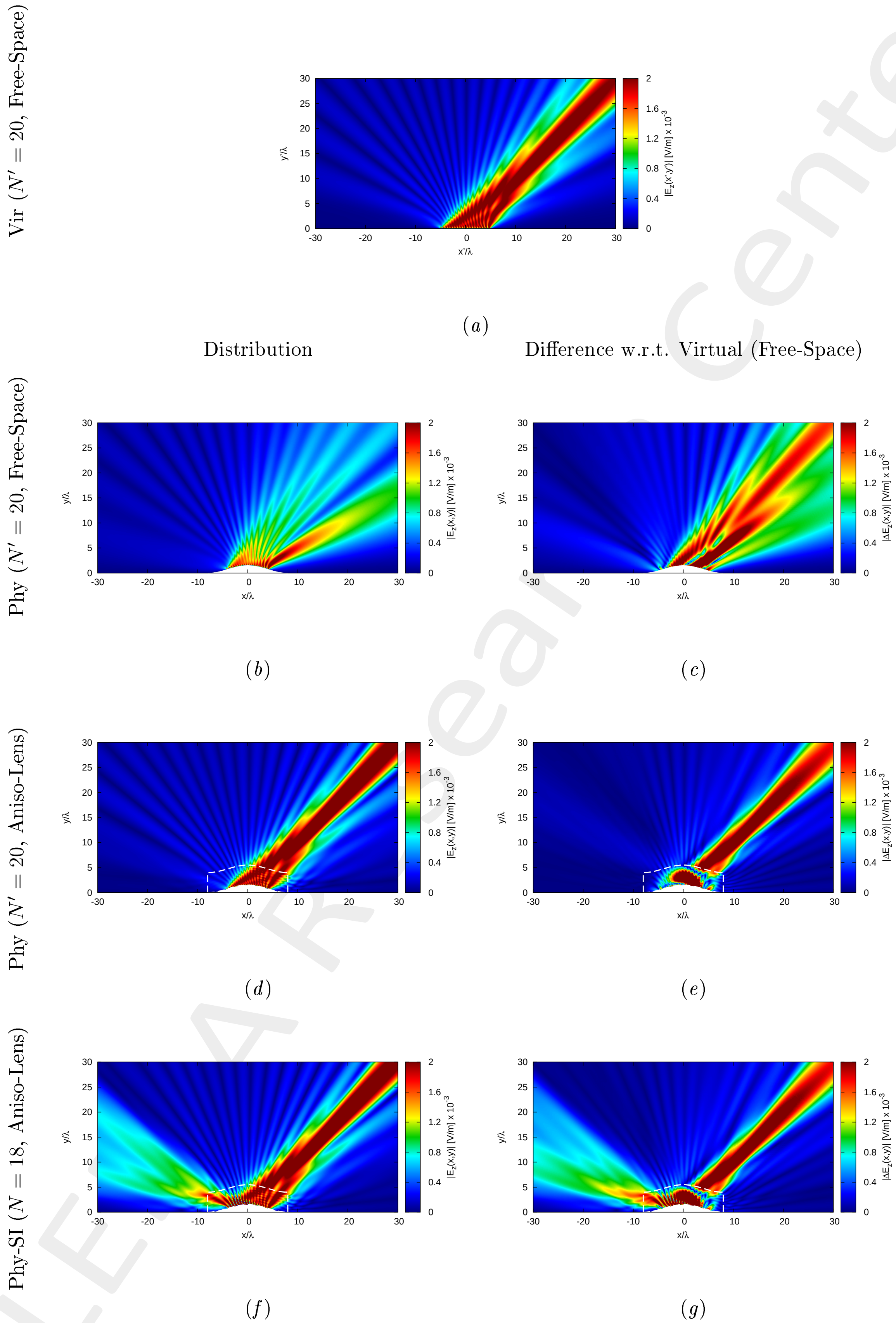

Figure 33: Lens Thickness $s = 4.0$ $[\lambda]$ - Electric field distributions.

Curvature $l = 2.0$ $[\lambda]$

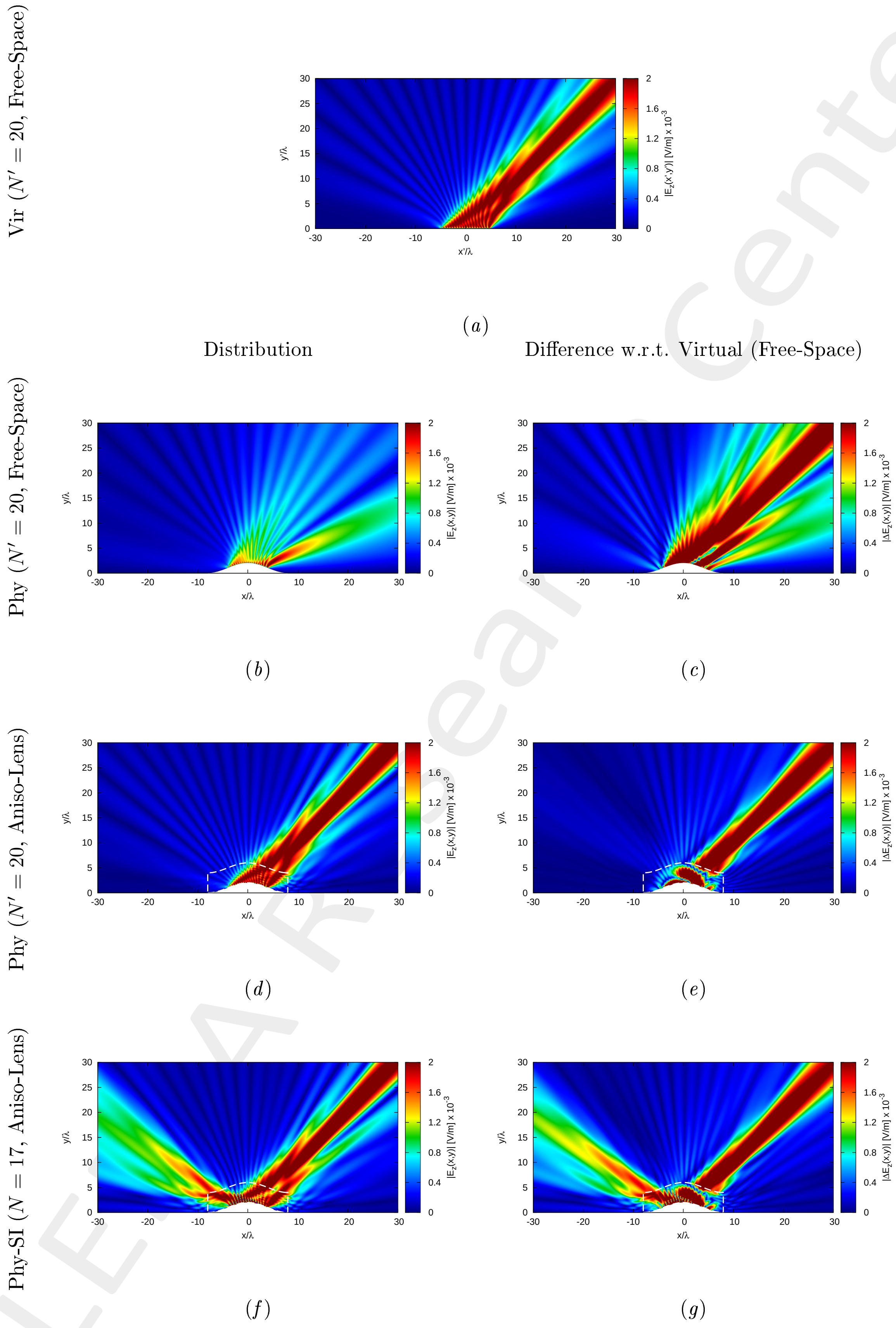

Figure 34: Lens Thickness $s = 4.0$ $[\lambda]$ - Electric field distributions.

1.2.7 Far-Field Patterns (Aniso-Lens, $\phi_s = 90.0$ $[deg]$)

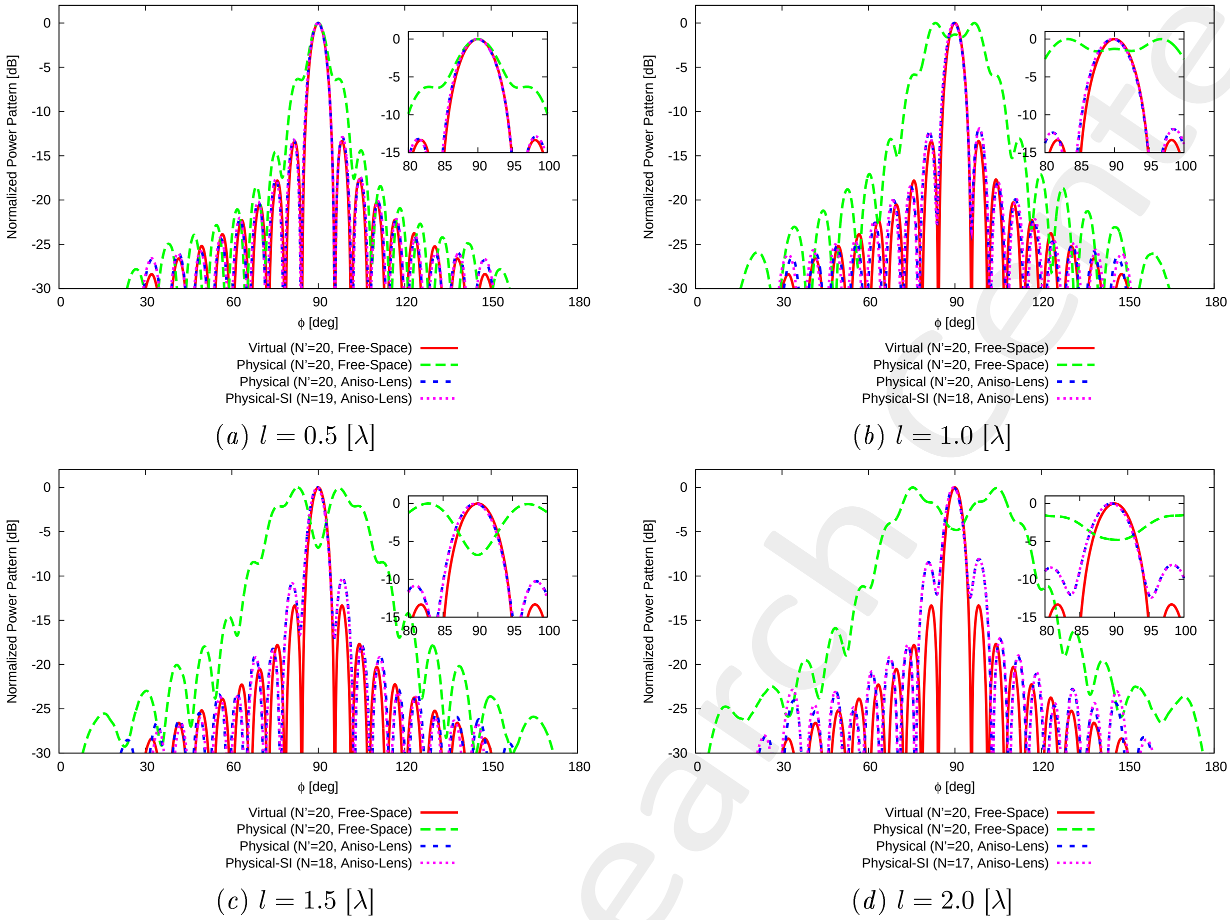

Figure 35: Lens thickness $s = 4.0$ $[\lambda]$ - Comparison between the far field patterns or different curvatures of the lens.

1.2.8 Far-Field Patterns (Aniso-Lens, $\phi_s = 75.0$ $[deg]$)

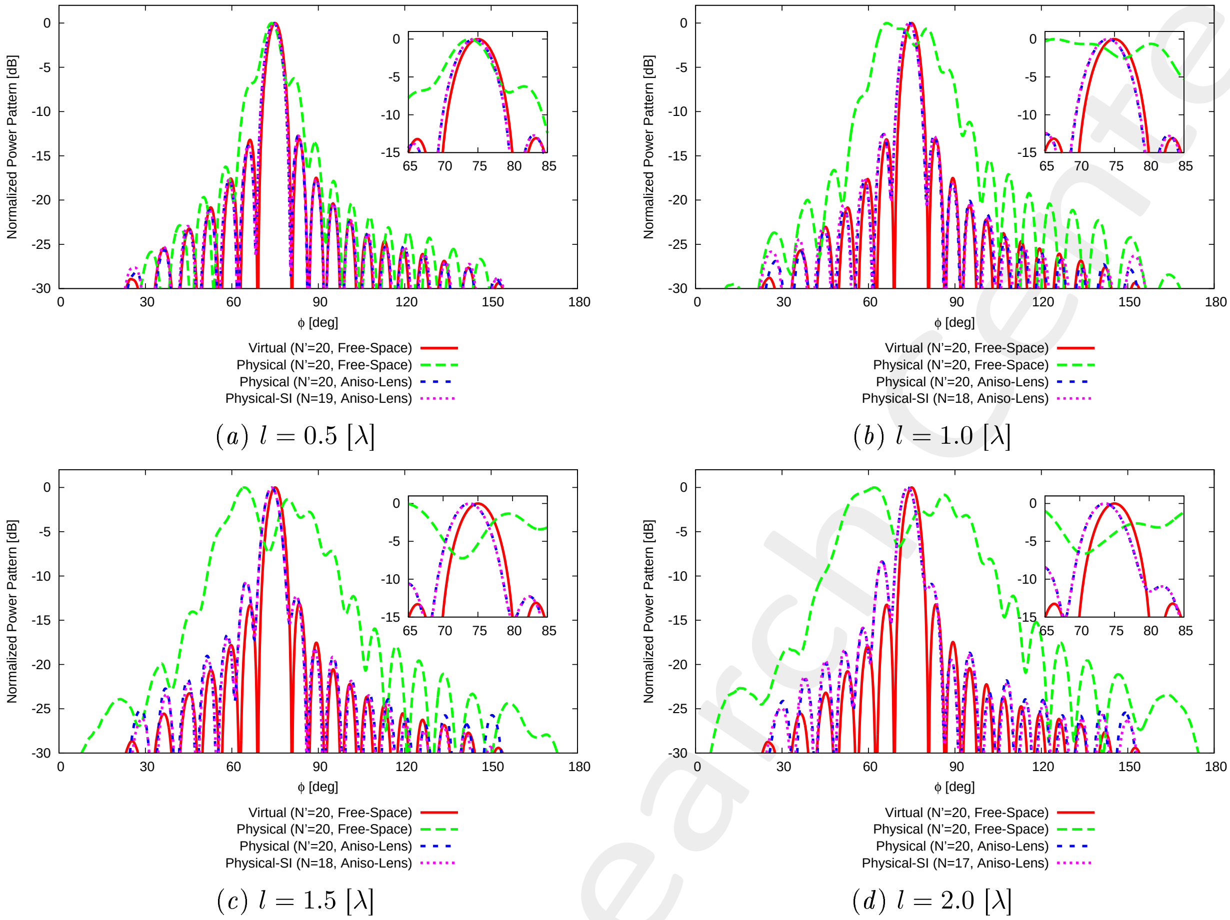

(a) $l = 0.5$ $[\lambda]$ (b) $l = 1.0$ $[\lambda]$ (c) $l = 1.5$ $[\lambda]$ (d) $l = 2.0$ $[\lambda]$

Figure 36: Lens thickness $s = 4.0$ $[\lambda]$ - Comparison between the far field patterns or different curvatures of the lens.

1.2.9 Far-Field Patterns (Aniso-Lens, $\phi_s = 60.0$ $[deg]$)

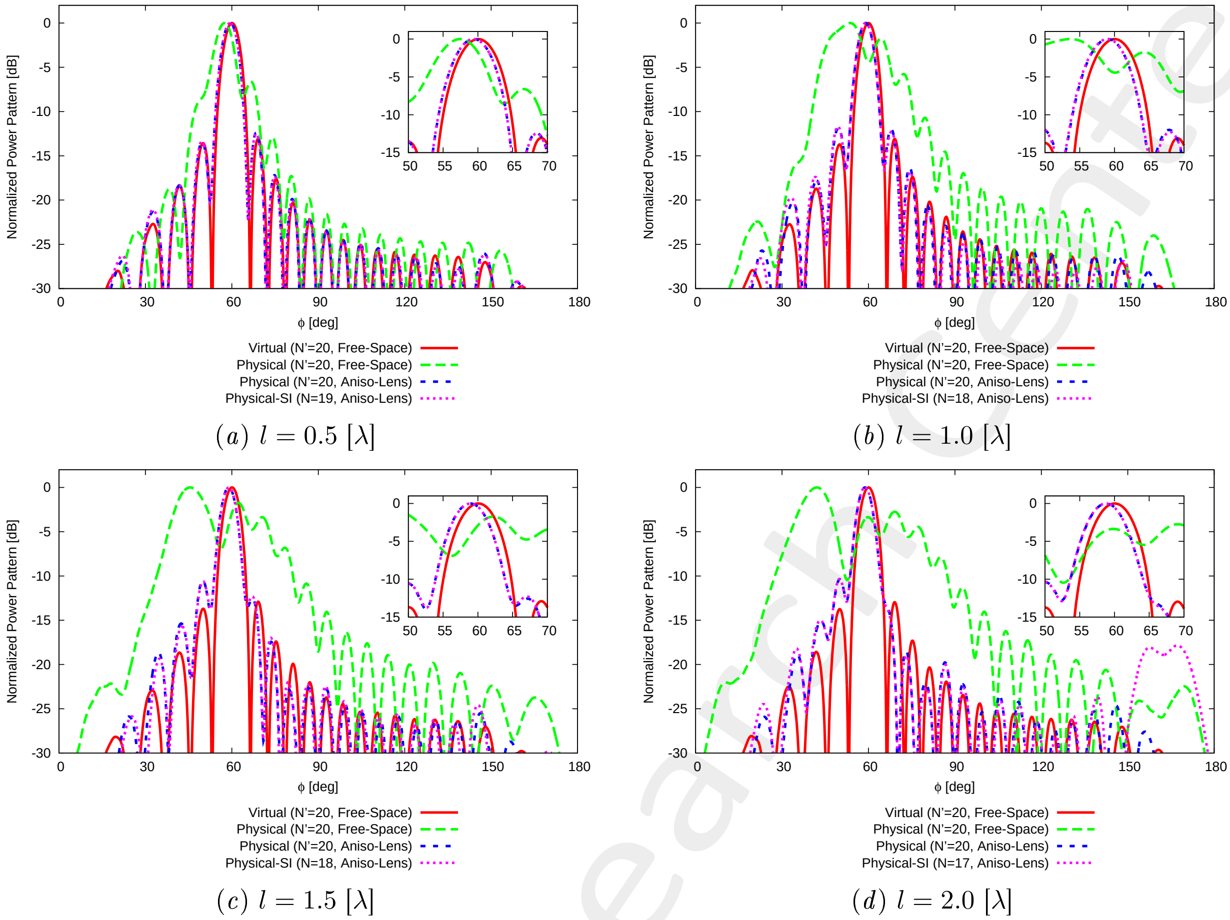

(a) $l = 0.5$ $[\lambda]$ (b) $l = 1.0$ $[\lambda]$ (c) $l = 1.5$ $[\lambda]$ (d) $l = 2.0$ $[\lambda]$

Figure 37: Lens thickness $s = 4.0$ $[\lambda]$ - Comparison between the far field patterns or different curvatures of the lens.

1.2.10 Far-Field Patterns (Aniso-Lens, $\phi_s = 45.0$ [deg])

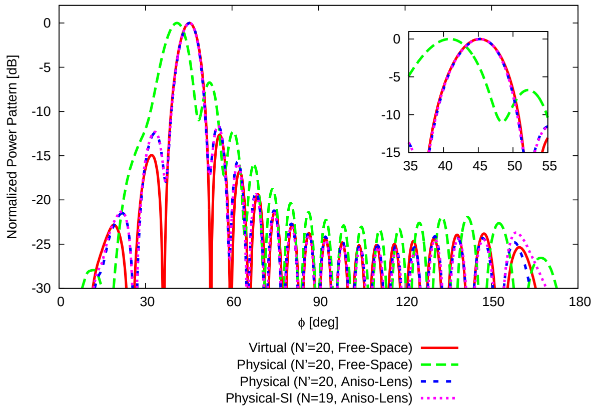

(a) $l = 0.5$ [λ]

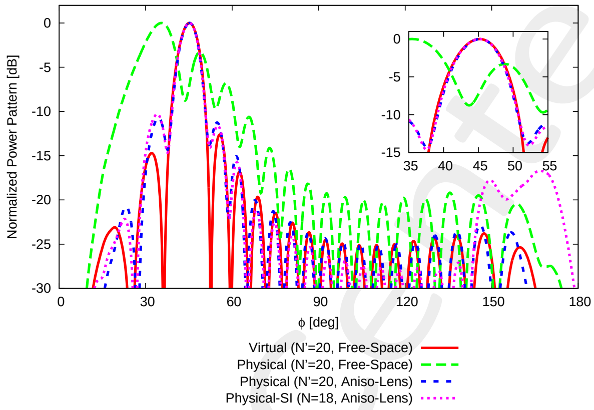

(b) $l = 1.0$ [λ]

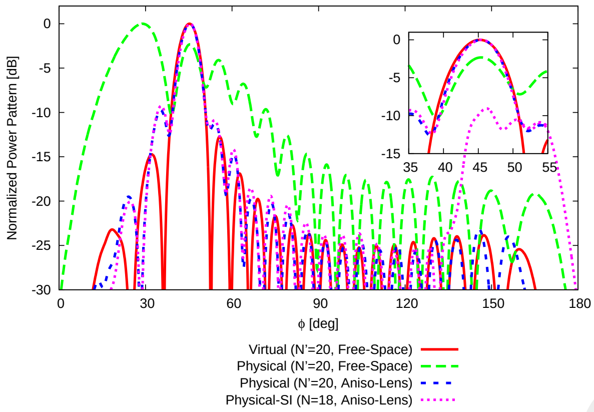

(c) $l = 1.5$ [λ]

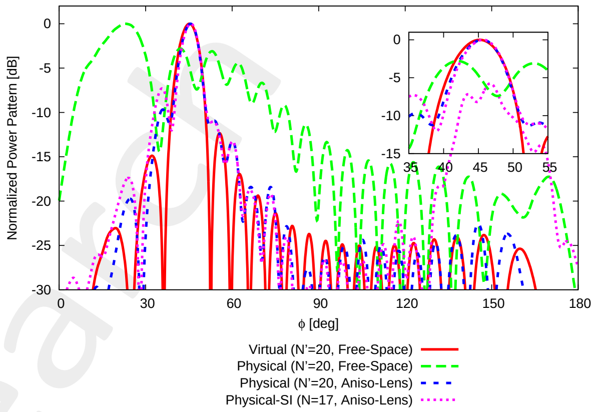

(d) $l = 2.0$ [λ]

Figure 38: Lens thickness $s = 4.0$ [λ] - Comparison between the far field patterns or different curvatures of the lens.

References

[1] G. Oliveri, G. Gottardi, F. Robol, A. Polo, L. Poli, M. Salucci, M. Chuan, C. Massagrande, P. Vinetti, M. Mattivi, R. Lombardi, and A. Massa, "Co-design of unconventional array architectures and antenna elements for 5G base station," *IEEE Trans. Antennas Propag.*, vol. 65, no. 12, pp. 6752-6767, Dec. 2017.

[2] P. Rocca, G. Oliveri, R. J. Mailloux, and A. Massa, "Unconventional phased array architectures and design methodologies - A review," *Proc. IEEE*, vol. 104, no. 3, pp. 544-560, Mar. 2016.

[3] G. Oliveri, M. Salucci, N. Anselmi and A. Massa, "Multiscale System-by-Design synthesis of printed WAIMs for waveguide array enhancement," *IEEE J. Multiscale Multiphysics Computat. Techn.*, vol. 2, pp. 84-96, 2017.

[4] A. Massa and G. Oliveri, "Metamaterial-by-Design: Theory, methods, and applications to communications and sensing - Editorial," *EPJ Applied Metamaterials*, vol. 3, no. E1, pp. 1-3, 2016.

[5] L. Poli, G. Oliveri, P. Rocca, M. Salucci, and A. Massa, "Long-Distance WPT Unconventional Arrays Synthesis," *J. Electromagnet. Waves Appl.*, vol. 31, no. 14, pp. 1399-1420, Jul. 2017.

[6] G. Oliveri, F. Viani, N. Anselmi, and A. Massa, "Synthesis of multi-layer WAIM coatings for planar phased arrays within the system-by-design framework," *IEEE Trans. Antennas Propag.*, vol. 63, no. 6, pp. 2482-2496, Jun. 2015.

[7] G. Oliveri, L. Tenuti, E. Bekele, M. Carlin, and A. Massa, "An SbD-QCTO approach to the synthesis of isotropic metamaterial lenses," *IEEE Antennas Wireless Propag. Lett.*, vol. 13, pp. 1783-1786, 2014.

[8] G. Oliveri, D. H. Werner, and A. Massa, "Reconfigurable electromagnetics through metamaterials - A review" *Proc. IEEE*, vol. 103, no. 7, pp. 1034-1056, Jul. 2015.

[9] G. Oliveri, E. T. Bekele, M. Salucci, and A. Massa, "Transformation electromagnetics miniaturization of sectoral and conical horn antennas," *IEEE Trans. Antennas Propag.*, vol. 64, no. 4, pp. 1508-1513, Apr. 2016.

[10] G. Oliveri, E. T. Bekele, M. Salucci, and A. Massa, "Array miniaturization through QCTO-SI metamaterial radomes," *IEEE Trans. Antennas Propag.*, vol. 63, no. 8, pp. 3465-3476, Aug. 2015.

[11] G. Oliveri, E. T. Bekele, D. H. Werner, J. P. Turpin, and A. Massa, "Generalized QCTO for metamaterial-lens-coated conformal arrays," *IEEE Trans. Antennas Propag.*, vol. 62, no. 8, pp 4089-4095, Aug. 2014.

[12] G. Oliveri, E. Bekele, M. Carlin, L. Tenuti, J. Turpin, D. H. Werner, and A. Massa, "Extended QCTO for innovative antenna system designs," IEEE Antenna Conference on Antenna Measurements and Applications (CAMA 2014), pp. 1-3, Nov. 16-19, 2014.

[13] G. Oliveri, P. Rocca, M. Salucci, E. T. Bekele, D. H. Werner, and A. Massa, "Design and synthesis of innovative metamaterial-enhanced arrays," IEEE International Symposium on Antennas Propag. (APS/URSI 2013), Orlando, Florida, USA, pp. 972 - 973, Jul. 7-12, 2013.

[14] G. Oliveri, “Improving the reliability of frequency domain simulators in the presence of homogeneous metamaterials - A preliminary numerical assessment,” *Progress In Electromagnetics Research*, vol. 122, pp. 497-518, 2012.

[15] M. Salucci, G. Oliveri, N. Anselmi, G. Gottardi, and A. Massa, "Performance enhancement of linear active electronically-scanned arrays by means of MbD-synthesized metalenses," *J. Electromagnet. Waves Appl.*, vol. 32, no. 8, pp. 927-955, 2018.

[16] M. Salucci, G. Oliveri, N. Anselmi, and A. Massa, “Material-by-design synthesis of conformal miniaturized linear phased arrays,” *IEEE Access* (doi: 10.1109/ACCESS.2018.2833199).